

Marchenko redatuming, imaging, and multiple elimination and their mutual relations

Kees Wapenaar¹, Joeri Brackenhoff², Marcin Dukalski³, Giovanni Meles⁴, Christian Reinicke⁵, Evert Slob¹, Myrna Staring⁶, Jan Thorbecke¹, Joost van der Neut¹, and Lele Zhang¹

ABSTRACT

With the Marchenko method, it is possible to retrieve Green's functions between virtual sources in the subsurface and receivers at the surface from reflection data at the surface and focusing functions. A macro model of the subsurface is needed to estimate the first arrival; the internal multiples are retrieved entirely from the reflection data. The retrieved Green's functions form the input for redatuming by multidimensional deconvolution (MDD). The redatumed reflection response is free of internal multiples related to the overburden. Alternatively, the redatumed response can be obtained by applying a second focusing function to the retrieved Green's functions. This process is called Marchenko redatuming by double focusing. It is more stable and better suited for an adaptive implementation than Marchenko redatuming by MDD, but it does not eliminate the multiples between the target and the overburden. An attractive efficient

alternative is plane-wave Marchenko redatuming, which retrieves the responses to a limited number of plane-wave sources at the redatuming level. In all cases, an image of the subsurface can be obtained from the redatumed data, free of the artifacts caused by internal multiples. Another class of Marchenko methods aims at eliminating the internal multiples from the reflection data, while keeping the sources and receivers at the surface. A specific characteristic of this form of multiple elimination is that it predicts and subtracts all orders of internal multiples with the correct amplitude, without needing a macro subsurface model. Like Marchenko redatuming, Marchenko multiple elimination can be implemented as an MDD process, a double dereverberation process, or an efficient plane-wave oriented process. We have systematically examined the different approaches to Marchenko redatuming, imaging, and multiple elimination using a common mathematical framework.

INTRODUCTION

Building on the autofocusing method of [Rose \(2001, 2002\)](#), [Broggini and Snieder \(2012\)](#) show how the Marchenko method can be used to retrieve the 1D Green's function between a virtual source in the subsurface and a receiver at the surface from the reflection response at the surface. Unlike in seismic interferometry

([Campillo and Paul, 2003](#); [Wapenaar, 2003](#); [Schuster et al., 2004](#); [Bakulin and Calvert, 2006](#); [Gouédard et al., 2008](#)), no physical receiver is needed at the position of the virtual source. The generalization of this Green's function retrieval method to 3D situations ([Wapenaar et al., 2014](#)) formed the basis for the development of Marchenko redatuming and imaging methods ([Behura et al., 2014](#); [Broggini et al., 2014](#)). The main characteristic of these

Manuscript received by the Editor 28 November 2020; revised manuscript received 25 March 2021; published ahead of production 19 May 2021; published online 7 September 2021.

¹Delft University of Technology, Department of Geoscience and Engineering, Stevinweg 1, Delft 2628 CN, The Netherlands. E-mail: c.p.a.wapenaar@tudelft.nl (corresponding author); e.c.slob@tudelft.nl; J.W.Thorbecke@tudelft.nl; jrvanderneut@yahoo.com; L.Zhang-1@tudelft.nl.

²Delft University of Technology, Department of Geoscience and Engineering, Stevinweg 1, Delft 2628 CN, The Netherlands and ETH Zürich, Department of Earth Sciences, Sonneggstrasse 5, Zürich 8092, Switzerland. E-mail: johannes.brackenhoff@erdw.ethz.ch.

³Aramco Overseas Company B.V., Informaticalaan 6-12, Delft 2628 ZD, The Netherlands. E-mail: Marcin.Dukalski@aramcooverseas.com.

⁴Delft University of Technology, Department of Geoscience and Engineering, Stevinweg 1, Delft 2628 CN, The Netherlands and University of Lausanne, Institute of Earth Sciences, Lausanne 1015, Switzerland. E-mail: giovanni.meles@unil.ch.

⁵Delft University of Technology, Department of Geoscience and Engineering, Stevinweg 1, Delft 2628 CN, The Netherlands and Aramco Overseas Company B.V., Informaticalaan 6-12, Delft 2628 ZD, The Netherlands. E-mail: chris.reinicke@aramcooverseas.com.

⁶Delft University of Technology, Department of Geoscience and Engineering, Stevinweg 1, Delft 2628 CN, The Netherlands and Fugro Innovation and Technology, Prismastraat 4, Nootdorp 2631 RT, The Netherlands. E-mail: m.staring@fugro.com.

© 2021 Society of Exploration Geophysicists. All rights reserved.

methods is that internal multiples are dealt with in a data-driven way. A subsurface image obtained with the Marchenko method is free of artifacts related to internal multiples. The required input consists of the reflection response at the surface (deconvolved for the seismic wavelet and free of surface-related multiples) and an estimate of the direct arrivals of the Green's functions. The latter can be obtained from a macro model of the subsurface. Hence, the required input is the same as that for standard redatuming and imaging of primary reflections; the information needed to deal with the internal multiples comes entirely from the reflection response at the surface.

Since the introduction of the Marchenko method in geophysics, many variants have been introduced. In the initial approach, redatuming was achieved by applying multidimensional deconvolution (MDD) to the down- and upgoing Green's functions retrieved with the Marchenko method (Broggini et al., 2014; Ravasi et al., 2016). To obtain a more stable method, suited for adaptive implementation, redatuming by double focusing was developed (van der Neut et al., 2015c; Staring et al., 2018). An important efficiency gain was achieved with the plane-wave Marchenko redatuming approach (Meles et al., 2018). In all of these approaches, sources and receivers are redatumed from the surface to virtual sources and receivers at one or more depth levels in the subsurface. This requires a macro model of the overburden. To make the Marchenko method less sensitive to the macro model, it was proposed to extrapolate the virtual sources and receivers upward to the acquisition surface (Meles et al., 2016; van der Neut and Wapenaar, 2016). This led to a class of Marchenko multiple elimination methods, that is, methods in which the sources and receivers stay at the surface while the internal multiples are eliminated from the data (Pereira et al., 2019; Zhang et al., 2019a, 2019b; Dukalski and de Vos, 2020; Elison et al., 2020; Meles et al., 2020; Staring et al., 2021).

In this paper, we discuss the different Marchenko methods in a systematic way, show their mutual relations, and discuss the specific properties of each method. By using a consistent way of presenting these methods, using a unified notation, we hope to convey the systematics of the many Marchenko methods currently available. The emphasis will be on explanations with cartoon-like figures. Numerical examples and field data applications can be found in the referenced literature.

It is impossible to discuss all existing Marchenko methods in a single paper. At various places, we include references for variants that are not discussed here. In particular, the discussion in this paper is restricted to acoustic methods for lossless media. For a discussion of the Marchenko method in dissipative media, we refer to Slob (2016), and for elastodynamic Marchenko methods to Wapenaar and Slob (2014), da Costa Filho et al. (2014), and Reinicke et al. (2020). Throughout the paper, we assume that the input data are properly sampled. For Marchenko methods that compensate for the effects of irregular sampling, see Haindl et al. (2018), Peng et al. (2019), and van IJsseldijk and Wapenaar (2021). Recent developments on the integration of the Marchenko method with full-waveform inversion are also beyond the scope of this paper. For this subject, we refer to Cui et al. (2020) and Shoja et al. (2020). Finally, note that all applications indicated in this paper are restricted to the seismic reflection method. For a discussion of the "homogeneous Green's function approach" for monitoring and forecasting the responses to induced seismic sources, we refer readers to Brackenhoff et al. (2019a, 2019b).

MARCHENKO REDATUMING AND IMAGING

Seismic redatuming is the process of virtually moving sources and/or receivers from the acquisition surface to a new depth level (or "datum plane") in the subsurface. Traditionally, this is done with one-way wavefield extrapolation operators (or "focusing operators") that account for primaries only (Berkhout, 1982; Berryhill, 1984). Classic wavefield extrapolation and redatuming methods that account for internal multiples exist (Wapenaar et al., 1987; Mulder, 2005), but they require a very detailed subsurface model. Redatuming methods that are based on seismic interferometry (Schuster et al., 2004; Bakulin and Calvert, 2006; van der Neut et al., 2011) do not need a subsurface model, but they require the presence of actual receivers at the depth level to which one wants to redatum the sources.

Broggini and Snieder (2012) show that, with the Marchenko method, the same can be achieved as with seismic interferometry, at least in 1D, without requiring actual receivers in the subsurface. This was the inspiration for the research into 3D Marchenko redatuming and imaging, which is extensively discussed in this section. Marchenko redatuming is a data-driven method to create virtual sources and receivers in the subsurface. It accounts for internal multiples in the overburden, it only needs a macro model of the overburden, and it does not require the presence of actual receivers in the subsurface.

Focusing functions

The focusing function plays an essential role in the Marchenko method. It is a 3D generalization of the "fundamental solution" in 1D scattering problems (Lamb, 1980). However, from the seismic perspective it can be seen as a generalization of the 3D focusing operator used in traditional redatuming, accounting for internal multiples. Here, we discuss its basic properties. In the "Retrieval of focusing functions" section, we show how it can be retrieved from the reflection response at the surface.

Consider a 3D inhomogeneous lossless acoustic medium, with propagation velocity $c(\mathbf{x})$ and mass density $\rho(\mathbf{x})$, where $\mathbf{x} = (x_1, x_2, x_3)$ is the Cartesian coordinate vector. Here, x_1 and x_2 are the horizontal coordinates, in the following denoted by vector $\mathbf{x}_H = (x_1, x_2)$; x_3 is the depth coordinate. For 2D situations, the coordinate vectors reduce to $\mathbf{x} = (x_1, x_3)$ and $\mathbf{x}_H = x_1$, respectively. The acquisition boundary at $x_3 = x_{3,0}$ is denoted as \mathbb{S}_0 . Throughout this paper, we assume that \mathbb{S}_0 is a transparent boundary and that the upper half-space is homogeneous. We choose a focal point $\mathbf{x}_A = (\mathbf{x}_{H,A}, x_{3,A})$ in the subsurface, with $\mathbf{x}_{H,A} = (x_{1,A}, x_{2,A})$ (or $\mathbf{x}_{H,A} = x_{1,A}$ in the 2D situation) and $x_{3,A} > x_{3,0}$, and we define a boundary \mathbb{S}_A at the focal depth $x_{3,A}$. We define a truncated version of the medium, which is identical to the actual medium above \mathbb{S}_A and reflection free below \mathbb{S}_A . We introduce the focusing function $f_1(\mathbf{x}, \mathbf{x}_A, t)$ (with t denoting time) in this truncated medium. It consists of a downgoing part $f_1^+(\mathbf{x}, \mathbf{x}_A, t)$ and an upgoing part $f_1^-(\mathbf{x}, \mathbf{x}_A, t)$ (the superscripts $+$ and $-$ refer to the propagation direction at the first coordinate vector, here \mathbf{x}). The downgoing focusing function $f_1^+(\mathbf{x}_S, \mathbf{x}_A, t)$, with \mathbf{x}_S at \mathbb{S}_0 , is defined such that $f_1^+(\mathbf{x}, \mathbf{x}_A, t)$ focuses at $\mathbf{x} = \mathbf{x}_A$ and $t = 0$ and continues as a diverging downgoing field into the reflection-free half-space below \mathbb{S}_A . The upgoing focusing function $f_1^-(\mathbf{x}_R, \mathbf{x}_A, t)$ is the response of the truncated medium to $f_1^+(\mathbf{x}_S, \mathbf{x}_A, t)$, observed at \mathbf{x}_R at \mathbb{S}_0 . The downgoing and upgoing functions are visualized in Figure 1a.

Note that downgoing and upgoing waves meet each other at interfaces in such a way that only the direct arrival of the focusing function, denoted by $f_{1,d}^+(\mathbf{x}, \mathbf{x}_A, t)$, reaches the focal point.

The propagation of the focusing function through the truncated medium, from \mathbb{S}_0 to \mathbb{S}_A , is formally described by

$$f_1^+(\mathbf{x}'_A, \mathbf{x}_A, t) = \int_{\mathbb{S}_0} d\mathbf{x}_S \int_0^\infty T(\mathbf{x}'_A, \mathbf{x}_S, t') f_1^+(\mathbf{x}_S, \mathbf{x}_A, t - t') dt', \quad (1)$$

for \mathbf{x}'_A at \mathbb{S}_A , where $T(\mathbf{x}'_A, \mathbf{x}_S, t)$ is the transmission response of the truncated medium. Throughout the paper, we assume that down- and upgoing fields are power-flux normalized (Frasier, 1970; Kennett et al., 1978; Ursin, 1983; Chapman, 1994), which explains why expressions such as equation 1 do not contain the vertical spatial derivative of one of the functions under the integral. The formal focusing conditions are

$$f_1^+(\mathbf{x}'_A, \mathbf{x}_A, t) = \delta(\mathbf{x}'_{H,A} - \mathbf{x}_{H,A}) \delta(t), \quad (2)$$

$$f_1^-(\mathbf{x}'_A, \mathbf{x}_A, t) = 0, \quad (3)$$

for \mathbf{x}'_A at \mathbb{S}_A . From equations 1 and 2, it follows that $f_1^+(\mathbf{x}_S, \mathbf{x}_A, t)$ is by definition the inverse of $T(\mathbf{x}_A, \mathbf{x}_S, t)$. For the truncated medium of Figure 1a, the downgoing function $f_1^+(\mathbf{x}_S, \mathbf{x}_A, t)$, convolved with a wavelet, is shown in gray-level display in Figure 1b. Its direct contribution $f_{1,d}^+(\mathbf{x}_S, \mathbf{x}_A, t)$ is a hyperbolic-like event at negative time (actually, this is the traditional one-way focusing operator [Berkhout and Wapenaar, 1993]). If no scattering occurred between \mathbb{S}_0 and \mathbb{S}_A , this would be the complete focusing function. However, in a scattering medium, additional events are present in $f_1^+(\mathbf{x}_S, \mathbf{x}_A, t)$ (as visualized in Figure 1a and 1b), which prevent that multiply scattered waves reach \mathbb{S}_A . Figure 1c shows the focused field $f_1^+(\mathbf{x}'_A, \mathbf{x}_A, t)$, with \mathbf{x}'_A at \mathbb{S}_A , obtained by emitting $f_1^+(\mathbf{x}_S, \mathbf{x}_A, t)$ (convolved with a wavelet) into the truncated medium, according to equation 1. The amplitudes are clipped to emphasize the details. Note that there are no artifacts related to multiple scattering. Nevertheless, the focused field deviates from the desired result, expressed by equation 2. The explanation is that, in practical situations, the aperture is finite and focusing functions do not compensate for evanescent waves, which implies a spatial band limitation (Berkhout and van Wulfften Palthe, 1979, Appendix C). Moreover, in practice, the seismic wavelet implies a temporal band limitation. Hence, the delta functions in equation 2 (and in the remainder of the paper) should be interpreted as band-limited delta functions. Consequently, in practice, the downgoing focusing function $f_1^+(\mathbf{x}_S, \mathbf{x}_A, t)$ is actually a band-limited inverse of the transmission response $T(\mathbf{x}_A, \mathbf{x}_S, t)$.

Representations

We discuss two representations, which formulate the mutual relations between the Green's functions and the focusing functions introduced in the previous section. First, we introduce the decomposed Green's functions $G^{-,+}(\mathbf{x}_R, \mathbf{x}_A, t)$ and $G^{-,-}(\mathbf{x}_R, \mathbf{x}_A, t)$, with \mathbf{x}_A at \mathbb{S}_A inside the medium and \mathbf{x}_R at the acquisition boundary \mathbb{S}_0 ; see Figure 2a. Unlike the focusing functions, the Green's functions are defined in the actual medium, which in general is inhomogeneous below \mathbb{S}_A . Following common conventions, the second coordinate vector (here \mathbf{x}_A) denotes the position of the impulsive source and the first coordinate vector (here \mathbf{x}_R) denotes that of the receiver. In the same order, the superscripts denote the propagation directions at the source and receiver. Because the half-space above \mathbb{S}_0 is homogeneous, only upgoing waves arrive at the receiver.

For a source at \mathbf{x}_S at the acquisition boundary \mathbb{S}_0 , the Green's function $G^{-,+}(\mathbf{x}_R, \mathbf{x}_S, t)$ is by definition the reflection response of the medium. We denote this by $R(\mathbf{x}_R, \mathbf{x}_S, t)$. The following relations hold between the power-flux normalized Green's functions and focusing functions (Slob et al., 2014; Wapenaar et al., 2014):

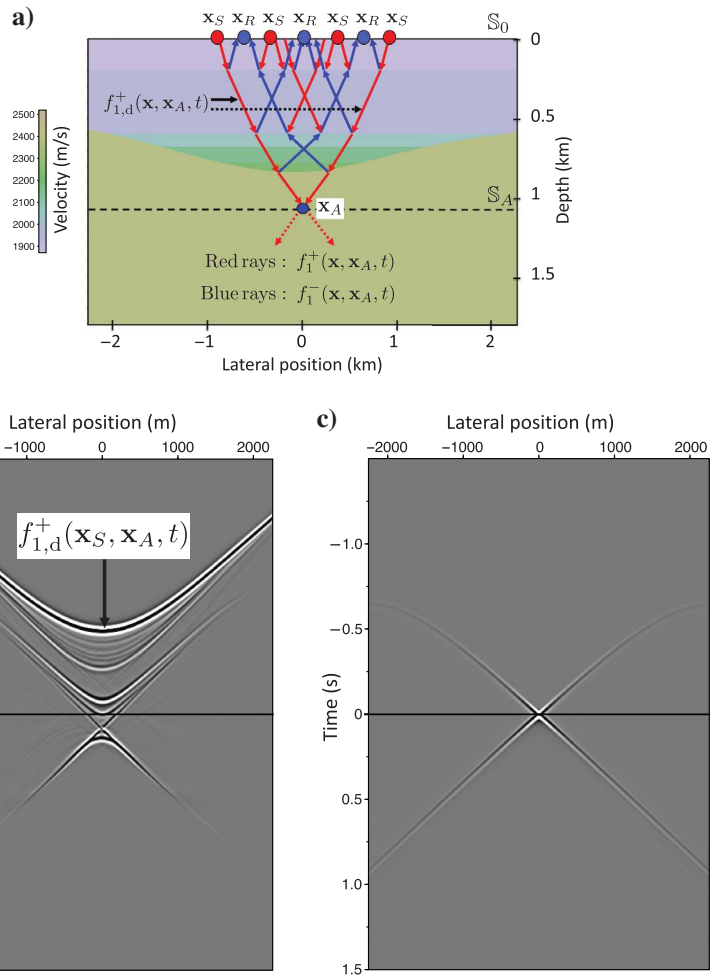


Figure 1. (a) Focusing functions f_1^+ and f_1^- in the truncated medium. (b) The focusing function $f_{1,d}^+(\mathbf{x}_S, \mathbf{x}_A, t)$ (fixed \mathbf{x}_A , variable \mathbf{x}_S) with \mathbf{x}_S at \mathbb{S}_0 and \mathbf{x}_A at \mathbb{S}_A . (c) The focused field $f_1^+(\mathbf{x}'_A, \mathbf{x}_A, t)$ (fixed \mathbf{x}_A , variable \mathbf{x}'_A) with \mathbf{x}'_A and \mathbf{x}_A at \mathbb{S}_A .

$$G^{-,+}(\mathbf{x}_R, \mathbf{x}_A, t) + f_1^-(\mathbf{x}_R, \mathbf{x}_A, t) = \int_{\mathbb{S}_0} d\mathbf{x}_S \int_0^\infty R(\mathbf{x}_R, \mathbf{x}_S, t') f_1^+(\mathbf{x}_S, \mathbf{x}_A, t - t') dt' \quad (4)$$

and

$$G^{-,-}(\mathbf{x}_R, \mathbf{x}_A, -t) + f_1^+(\mathbf{x}_R, \mathbf{x}_A, t) = \int_{\mathbb{S}_0} d\mathbf{x}_S \int_{-\infty}^0 R(\mathbf{x}_R, \mathbf{x}_S, -t') f_1^-(\mathbf{x}_S, \mathbf{x}_A, t - t') dt'. \quad (5)$$

The time integration boundaries acknowledge the fact that the reflection response $R(\mathbf{x}_R, \mathbf{x}_S, t)$ is a causal function of time, that is, $R(\mathbf{x}_R, \mathbf{x}_S, t < 0) = 0$. Both equations account for internal multiple scattering. Equation 4 is exact, whereas in equation 5 evanescent waves are neglected. The interpretation of equation 4 is as follows. The right side quantifies the reflection response of the actual medium to the downgoing focusing function $f_1^+(\mathbf{x}_S, \mathbf{x}_A, t)$. The left side shows that this reflection response consists of the upgoing focusing function $f_1^-(\mathbf{x}_R, \mathbf{x}_A, t)$ (the blue rays arriving at \mathbb{S}_0 in Figure 1a) and the Green's function $G^{-,+}(\mathbf{x}_R, \mathbf{x}_A, t)$. The latter can be understood as follows. In Figure 1a, it can be seen that

the focal point \mathbf{x}_A acts as a virtual source at $t = 0$ for downgoing waves. Figure 2a shows that the response to this virtual source is the Green's function $G^{-,+}(\mathbf{x}_R, \mathbf{x}_A, t)$ (the green rays in this figure). Equation 5 is interpreted in a similar way. The right side quantifies the reflection response of the time-reversed actual medium to the upgoing focusing function $f_1^-(\mathbf{x}_S, \mathbf{x}_A, t)$. The left side shows that this reflection response consists of the downgoing focusing function $f_1^+(\mathbf{x}_R, \mathbf{x}_A, t)$ and the time-reversed Green's function $G^{-,-}(\mathbf{x}_R, \mathbf{x}_A, -t)$. The functions on the left sides of equations 4 and 5, convolved with a wavelet, are shown in gray-level display in Figure 2b and 2c, respectively.

Recall that we assume that \mathbb{S}_0 is a transparent boundary and that the half-space above \mathbb{S}_0 is homogeneous. Hence, the reflection response R in equations 4 and 5 contains no surface-related multiples, which complies with the situation after surface-related multiple elimination (Verschuur et al., 1992; van Groenestijn and Verschuur, 2010). Alternatively, equations 4 and 5 can be modified to account for surface-related multiples in R (see Ware and Aki [1969] for the 1D situation and Singh et al. [2017] and Dukalski and de Vos [2018] for 2D and 3D situations). A further discussion on the inclusion of surface-related multiples in the representations is beyond the scope of this paper.

Retrieval of focusing functions

Assuming that R is known, equations 4 and 5 form a system of two equations for four unknowns (f_1^+ , f_1^- , $G^{-,+}$, and $G^{-,-}$). An inspection of Figure 2b and 2c reveals that the Green's functions reside in other time intervals than the focusing functions. We discuss window functions to suppress the Green's functions from equations 4 and 5, so that we are left with a system of two equations for two unknowns. To define a time window for equation 4, we need to know the first possible arrival of $G^{-,+}(\mathbf{x}_R, \mathbf{x}_A, t)$. This would occur when there would be a reflector just below \mathbb{S}_A . For the first possible arrival of this Green's function, we write

$$\{G^{-,+}(\mathbf{x}_R, \mathbf{x}_A, t)\}^{\text{first}} \propto T_d(\mathbf{x}_R, \mathbf{x}_A, t), \quad (6)$$

where "first" stands for "first possible," T_d is the direct arrival of the transmission response of the medium between \mathbb{S}_A and \mathbb{S}_0 (which is also the direct arrival of $G^{-,-}$; see Figure 2a), and \propto stands for "proportional to." Note that we ignored the reflection coefficient of the hypothetical reflector (this is justified because we only use equation 6 to derive the time window). We denote the arrival time of the direct transmission response as $t_d(\mathbf{x}_R, \mathbf{x}_A)$. Hence, $G^{-,+}(\mathbf{x}_R, \mathbf{x}_A, t)$ can be suppressed from equation 4 by applying a time window that removes everything beyond $t = t_b = t_d(\mathbf{x}_R, \mathbf{x}_A) - \epsilon$ (the dashed line in Figure 2b). Here, ϵ is a small positive time constant (typically half the duration of a wavelet), to account for the fact that, in practice, all terms in equations 4 and 5 are band limited. To define a

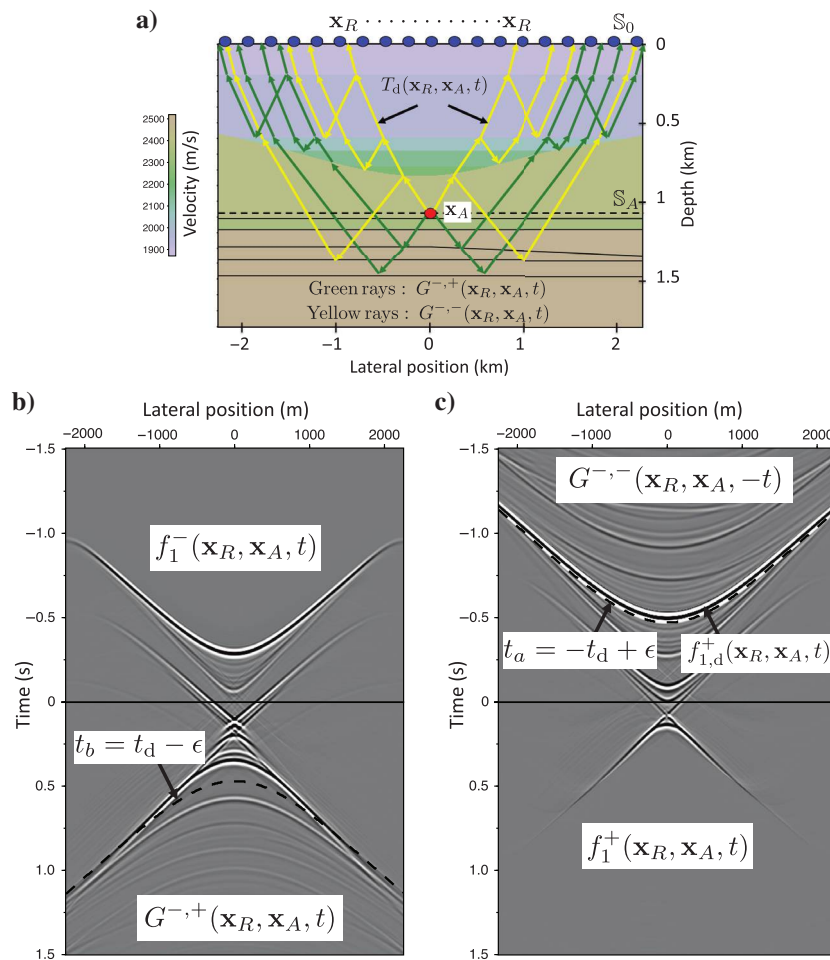


Figure 2. (a) Green's functions in the actual medium. (b) The left side of equation 4 (fixed \mathbf{x}_A , variable \mathbf{x}_R). (c) The left side of equation 5.

time window for equation 5, we need to know the last arrival of the time-reversed Green's function $G^{-\cdot}(\mathbf{x}_R, \mathbf{x}_A, -t)$. This is given by the time-reversed direct arrival; hence,

$$\{G^{-\cdot}(\mathbf{x}_R, \mathbf{x}_A, -t)\}_{\text{last}} = -T_d(\mathbf{x}_R, \mathbf{x}_A, -t) \quad (7)$$

(the factor -1 follows from the sign-convention for the source for upgoing waves in $G^{-\cdot}$ [Wapenaar, 1996], but this sign is irrelevant for the derivation of the time window). Hence, $G^{-\cdot}(\mathbf{x}_R, \mathbf{x}_A, -t)$ can be suppressed from equation 5 by applying a time window that removes everything before $t = t_a = -t_d(\mathbf{x}_R, \mathbf{x}_A) + \epsilon$ (the dashed line in Figure 2c). Note that $t_a = -t_b$. Based on this analysis, we define two time windows as

$$\Theta_a(\mathbf{x}_R, \mathbf{x}_A, t) = \theta(t - t_a) = \theta(t + t_d - \epsilon), \quad (8)$$

$$\Theta_b(\mathbf{x}_R, \mathbf{x}_A, t) = \theta(t_b - t) = \theta(t_d - \epsilon - t), \quad (9)$$

where $\theta(t)$ is the Heaviside step function (or, in practice, a tapered version of the Heaviside step function). These windows suppress the Green's functions and pass the focusing functions f_1^+ and f_1^- , except the direct arrival $f_{1,d}^+(\mathbf{x}_R, \mathbf{x}_A, t)$, which coincides with the last arrival of $G^{-\cdot}(\mathbf{x}_R, \mathbf{x}_A, -t)$; see Figure 2c.

Here, a few words of caution are needed. First, equation 6 is only correct for limited offsets: At large offsets, refracted waves in $G^{-\cdot}$ may arrive earlier than T_d . Second, in a laterally varying strongly scattering medium, diffraction events in the focusing functions may be unintentionally suppressed by the time windows. Third, in practice, the inherent band limitation may cause partial interference of focusing functions and Green's functions, particularly in the case of thin layers (i.e., thin compared to the wavelength). In this paper, we assume that offsets are limited, lateral variations are mild, and layers are not thin. Dukalski et al. (2019) discuss how to account for thin layering, assuming that the medium is horizontally layered.

Application of the window $\Theta_b(\mathbf{x}_R, \mathbf{x}_A, t)$ to both sides of equation 4 gives

$$f_1^-(\mathbf{x}_R, \mathbf{x}_A, t) = \Theta_b \int_{\mathbb{S}_0} d\mathbf{x}_S \int_0^\infty R(\mathbf{x}_R, \mathbf{x}_S, t') f_1^+(\mathbf{x}_S, \mathbf{x}_A, t - t') dt'. \quad (10)$$

Similarly, applying $\Theta_a(\mathbf{x}_R, \mathbf{x}_A, t)$ to both sides of equation 5 we obtain

$$\begin{aligned} f_1^+(\mathbf{x}_R, \mathbf{x}_A, t) - f_{1,d}^+(\mathbf{x}_R, \mathbf{x}_A, t) \\ = \Theta_a \int_{\mathbb{S}_0} d\mathbf{x}_S \int_{-\infty}^0 R(\mathbf{x}_R, \mathbf{x}_S, -t') f_1^-(\mathbf{x}_S, \mathbf{x}_A, t - t') dt'. \end{aligned} \quad (11)$$

The term $-f_{1,d}^+$ on the left side of equation 11 accounts for the fact that $f_{1,d}^+$ is not passed by the window; see Figure 2c. Equations 10 and 11 form a coupled system of Marchenko equations. We show how f_1^+ and f_1^- can be retrieved, assuming that R and $f_{1,d}^+$ are known. We adopt the compact operator notation introduced by van der Neut et al. (2015b). In this notation, equations 10 and 11 read

$$f_1^- = \Theta_b R f_1^+, \quad (12)$$

$$f_1^+ = \Theta_a R^* f_1^- + f_{1,d}^+, \quad (13)$$

with superscript \star denoting time reversal. For simplicity, we use the same fonts for operators as for wavefields. Operations like $R f_1^+$ stand for a (multidimensional) convolution process (see the right side of equation 10), whereas operations containing a time reversal, such as $R^* f_1^-$, stand for a correlation process (see the right side of equation 11). Window functions are always applied in a multiplicative sense. Substitution of equation 12 into equation 13 gives

$$f_1^+ = \Theta_a R^* \Theta_b R f_1^+ + f_{1,d}^+, \quad (14)$$

The product notation $\Theta_a R^* \Theta_b R f_1^+$ should be understood in the sense that operators and window functions act on all terms to the right of it; hence, it stands for $\Theta_a (R^* (\Theta_b (R f_1^+)))$. For notational convenience, we will not use the brackets. We rewrite equation 14 as

$$\{\delta - \Theta_a R^* \Theta_b R\} f_1^+ = f_{1,d}^+, \quad (15)$$

where δ is the identity operator. This equation can be solved by

$$f_1^+ = \sum_{k=0}^K \{\Theta_a R^* \Theta_b R\}^k f_{1,d}^+, \quad (16)$$

where K is the number of iterations needed for the scheme to converge with acceptable accuracy (the convergence is guaranteed for $K \rightarrow \infty$ [Dukalski and de Vos, 2018]). Other approaches to solve equation 15 are proposed by van der Neut et al. (2015a), Dukalski and de Vos (2018), and Becker et al. (2018). Once f_1^+ is found, f_1^- follows from equation 12. We call equation 16 the Marchenko scheme. As input, it requires the reflection response $R(\mathbf{x}_R, \mathbf{x}_S, t)$ at the acquisition boundary (i.e., the reflection measurements after surface-related multiple elimination and deconvolution for the wavelet) and the direct arrival $f_{1,d}^+(\mathbf{x}_R, \mathbf{x}_A, t)$ of the focusing function. Analogous to equations 1 and 2, the latter is related to the direct arrival of the transmission response via

$$\delta(\mathbf{x}'_{H,A} - \mathbf{x}_{H,A}) \delta(t) = \int_{\mathbb{S}_0} d\mathbf{x}_R \int_0^\infty T_d(\mathbf{x}'_A, \mathbf{x}_R, t') f_{1,d}^+(\mathbf{x}_R, \mathbf{x}_A, t - t') dt', \quad (17)$$

for \mathbf{x}_A and \mathbf{x}'_A at \mathbb{S}_A . Hence, $f_{1,d}^+(\mathbf{x}_R, \mathbf{x}_A, t)$ is the (in practice, band limited) inverse of $T_d(\mathbf{x}_A, \mathbf{x}_R, t)$. When a macro model of the medium between \mathbb{S}_0 and \mathbb{S}_A is available, T_d can be derived from this model and inverted to obtain $f_{1,d}^+$. For convenience, this inversion is often approximated by time reversal, according to $f_{1,d}^+(\mathbf{x}_R, \mathbf{x}_A, t) \approx T_d(\mathbf{x}_A, \mathbf{x}_R, -t)$. The Marchenko scheme appears to be quite robust with respect to amplitude and timing errors in the direct arrival of the focusing function (Broggini et al., 2014; Wapenaar et al., 2014). Nevertheless, for horizontally layered media, the amplitude of the direct arrival can be corrected, using the principle of energy conservation (Mildner et al., 2019). For highly complex media, it can be advantageous to account for wavefield complexity in the initial estimate of the focusing function

(Vasconcelos et al., 2015; Vasconcelos and Sripanich, 2019). In the “Marchenko multiple elimination” section, we discuss methods that are independent of the direct arrival of the focusing function.

Retrieval of Green’s functions (source redatuming)

Once the focusing functions have been found, the next step is retrieval of the Green’s functions. We define time windows $\Psi_a(\mathbf{x}_R, \mathbf{x}_A, t)$ and $\Psi_b(\mathbf{x}_R, \mathbf{x}_A, t)$ via

$$\Psi_{a,b}(\mathbf{x}_R, \mathbf{x}_A, t) = 1 - \Theta_{a,b}(\mathbf{x}_R, \mathbf{x}_A, t). \quad (18)$$

Note that the windows $\Psi_{a,b}(\mathbf{x}_R, \mathbf{x}_A, t)$ are complementary to $\Theta_{a,b}(\mathbf{x}_R, \mathbf{x}_A, t)$, defined in equations 8 and 9. Hence, they pass the Green’s functions and suppress the focusing functions, except $f_{1,d}^+$; see Figure 2c. Application of $\Psi_b(\mathbf{x}_R, \mathbf{x}_A, t)$ to both sides of equation 4 thus gives

$$G^{-,+}(\mathbf{x}_R, \mathbf{x}_A, t) = \Psi_b \int_{\mathbb{S}_0} d\mathbf{x}_S \int_0^\infty R(\mathbf{x}_R, \mathbf{x}_S, t') f_1^+(\mathbf{x}_S, \mathbf{x}_A, t - t') dt'. \quad (19)$$

Similarly, applying $\Psi_a(\mathbf{x}_R, \mathbf{x}_A, t)$ to both sides of equation 5 yields

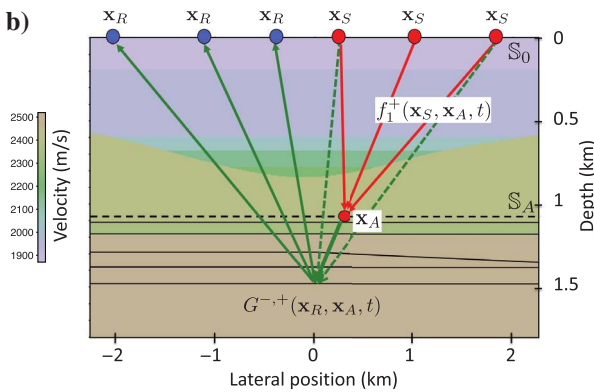
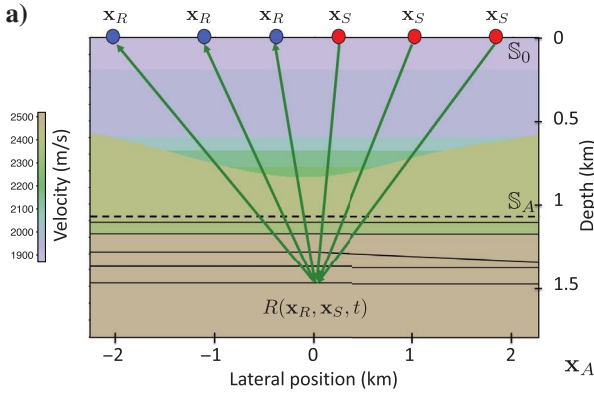


Figure 3. (a) Reflection response at the surface. Only a few rays are shown, mainly to indicate in which direction a wave leaves a source and arrives at a receiver, but note that the reflection response includes all primary and internal multiple reflections. (b) Visualization of equation 19 (source redatuming). The red rays indicate the focusing function (shown in more detail in Figure 1a), and the solid green rays represent the Green’s function (shown in more detail in Figure 2a).

$$\begin{aligned} & G^{-,-}(\mathbf{x}_R, \mathbf{x}_A, -t) + f_{1,d}^+(\mathbf{x}_R, \mathbf{x}_A, t) \\ &= \Psi_a \int_{\mathbb{S}_0} d\mathbf{x}_S \int_{-\infty}^0 R(\mathbf{x}_R, \mathbf{x}_S, -t') f_1^-(\mathbf{x}_S, \mathbf{x}_A, t - t') dt'. \end{aligned} \quad (20)$$

We interpret these expressions as follows. The reflection response on the right sides is the response to an actual source at \mathbf{x}_S , observed by an actual receiver at \mathbf{x}_R , both at the acquisition surface \mathbb{S}_0 . This is visualized in Figure 3a. The Green’s functions on the left sides are responses to a virtual source for downgoing waves (equation 19) and upgoing waves (equation 20) at \mathbf{x}_A in the subsurface, observed by the actual receiver at \mathbf{x}_R at the surface. Hence, equations 19 and 20 accomplish source redatuming from \mathbf{x}_S at the acquisition surface \mathbb{S}_0 to virtual-source position \mathbf{x}_A in the subsurface. Figure 3b visualizes equation 19.

Equation 19 and Figure 3b resemble the virtual-source method proposed by Bakulin and Calvert (2006), except that in their formulation the actual receivers are situated in a horizontal borehole and, instead of using a Marchenko-derived focusing function, they use a windowed time-reversed response between sources at the surface and an actual receiver at \mathbf{x}_A in the borehole. Hence, when measurements are available in a borehole, their method enables the retrieval of the response to a virtual source at \mathbf{x}_A below a complex overburden. Note, however, that their method does not account for internal multiples.

In the compact operator notation, equations 19 and 20 for source redatuming become

$$G_{R,A}^{-,+} = \Psi_b R f_1^+, \quad (21)$$

$$G_{R,A}^{-,-*} = \Psi_a R^* f_1^- - f_{1,d}^+, \quad (22)$$

where the subscripts R and A on the left sides refer to the actual receiver position \mathbf{x}_R at the surface \mathbb{S}_0 and the virtual-source position \mathbf{x}_A at the datum plane \mathbb{S}_A in the subsurface. In the following, we discuss different methods to redatum also the receivers from the surface to a virtual-receiver position \mathbf{x}_B at \mathbb{S}_A .

Receiver redatuming by MDD

We define the reflection response at datum plane \mathbb{S}_A of the target below \mathbb{S}_A as $R_{\text{tar}}(\mathbf{x}_B, \mathbf{x}_A, t) = G^{-,+}(\mathbf{x}_B, \mathbf{x}_A, t)$, with \mathbf{x}_A and \mathbf{x}_B at \mathbb{S}_A (the subscript “tar” stands for “target”). Note that, when $G^{-,+}(\mathbf{x}_B, \mathbf{x}_A, t)$ is defined in the actual medium, it not only contains the response of the medium below \mathbb{S}_A , but also multiples between reflectors below and above \mathbb{S}_A (the dashed rays in Figure 4a). We define a truncated medium, which is identical to the actual medium below \mathbb{S}_A and reflection free above \mathbb{S}_A (note that this is complementary to the truncated medium in which the focusing functions are defined). We denote the reflection response at \mathbb{S}_A of this truncated medium as $\bar{R}_{\text{tar}}(\mathbf{x}_B, \mathbf{x}_A, t) = \bar{G}^{-,+}(\mathbf{x}_B, \mathbf{x}_A, t)$. Obviously, this response does not contain the kind of multiples mentioned previously (Figure 4b).

The target reflection response $\bar{R}_{\text{tar}}(\mathbf{x}_B, \mathbf{x}_A, t)$ and the virtual-source responses defined in equations 19 and 20 are mutually related via

$$G^{-,+}(\mathbf{x}_R, \mathbf{x}_A, t) = - \int_{\mathbb{S}_A} d\mathbf{x}_B \int_0^t G^{-,-}(\mathbf{x}_R, \mathbf{x}_B, t') \bar{R}_{\text{tar}}(\mathbf{x}_B, \mathbf{x}_A, t - t') dt' \quad (23)$$

(Wapenaar, 1996; Amundsen, 2001; Reinicke et al., 2020). This relation is visualized in Figure 4c. The finite time integration interval follows from the fact that both quantities under the integral are causal functions of time. Equation 23 describes a multidimensional convolution, along time and space. Hence, resolving the target reflection response $\bar{R}_{\text{tar}}(\mathbf{x}_B, \mathbf{x}_A, t)$ from this equation is an MDD process, which redatums the receivers from \mathbb{S}_0 to \mathbb{S}_A . We thus obtain the redatumed reflection response $\bar{R}_{\text{tar}}(\mathbf{x}_B, \mathbf{x}_A, t)$, with its virtual source at \mathbf{x}_A and its virtual receiver at \mathbf{x}_B , both at \mathbb{S}_A . In principle, all effects of the overburden, including its internal multiple reflections, are completely removed by the redatuming process. For a field data application, we refer readers to Ravasi et al. (2016).

This MDD redatuming method resembles a process called rigorous redatuming, proposed by Mulder (2005), which also retrieves the target reflection response $\bar{R}_{\text{tar}}(\mathbf{x}_B, \mathbf{x}_A, t)$ from the reflection data at the surface. This method requires an accurate model of the medium between \mathbb{S}_0 and \mathbb{S}_A , explaining the primaries and the internal multiples. Contrarily, the Marchenko-based method only needs a macro model that explains the direct transmission response T_d between \mathbb{S}_0 and \mathbb{S}_A . The information needed to explain the internal multiples comes directly from the reflection response at the surface; see equation 16.

In the compact operator notation, equation 23 becomes

$$G_{R,A}^{-,+} = -G_{R,B}^{-,-} \bar{R}_{\text{tar}}. \quad (24)$$

In this notation, receiver redatuming by MDD is formally described by

$$\bar{R}_{\text{tar}} = -(G_{R,B}^{-,-})^{-1} G_{R,A}^{-,+}. \quad (25)$$

Note that $G_{R,A}^{-,+}$ and $G_{R,B}^{-,-}$ depend linearly on $f_{1,d}^+$ (see equations 12, 16, 21, and 22). Hence, amplitude errors in $f_{1,d}^+$ are for the larger part canceled in redatuming by MDD. This cancellation is complete when the medium is horizontally layered; it is approximate in a laterally varying medium. The redatumed response $\bar{R}_{\text{tar}}(\mathbf{x}_B, \mathbf{x}_A, t)$ is free of internal multiples related to the overburden and can be used as the input for imaging the target zone, for example, by standard reverse time migration (RTM). Although this does not remove internal multiples in the target zone, it yields a significant improvement over applying RTM to the reflection response at the surface. We refer readers to Broggin et al. (2014) for numerical examples.

Instead of inverting $G_{R,B}^{-,-}$, the target response \bar{R}_{tar} can be resolved directly from equation 24 by recasting the problem in terms of linear operators, which avoids the stabilization of $(G_{R,B}^{-,-})^{-1}$ needed in equation 25 (Luiken and van Leeuwen, 2020).

The redatuming method that we discuss in the next section is based on an explicit expression for R_{tar} and is therefore better equipped for practical applications.

Source and receiver redatuming by double focusing

Consider again equation 19, which describes source redatuming. Receiver redatuming can be formulated in a similar way, according to

$$R_{\text{tar}}(\mathbf{x}_B, \mathbf{x}_A, t) = \int_{\mathbb{S}_0} d\mathbf{x}_R \int_0^\infty f_1^+(\mathbf{x}_R, \mathbf{x}_B, t-t') G^{-,+}(\mathbf{x}_R, \mathbf{x}_A, t') dt' \quad (26)$$

(van der Neut et al., 2017; Wapenaar et al., 2019), where $R_{\text{tar}}(\mathbf{x}_B, \mathbf{x}_A, t) = G^{-,+}(\mathbf{x}_B, \mathbf{x}_A, t)$, with \mathbf{x}_A and \mathbf{x}_B at \mathbb{S}_A . The Green's function under the integral, $G^{-,+}(\mathbf{x}_R, \mathbf{x}_A, t)$, is the output of equation 19, which describes how the actual sources at \mathbf{x}_S are focused onto the virtual source at \mathbf{x}_A ; see Figure 3b. Similarly, equation 26 describes how the actual receivers at \mathbf{x}_R are focused onto the virtual receiver at \mathbf{x}_B ; see Figure 5. Hence, the combination of equations 19 and 26 can be seen as a double-focusing process, which is also clearly seen in Figure 5. Note that the redatumed response $R_{\text{tar}}(\mathbf{x}_B, \mathbf{x}_A, t)$ is defined in the actual medium; hence, apart from the response of the target below \mathbb{S}_A , it also contains multiples between reflectors below and above \mathbb{S}_A . This can be seen as a

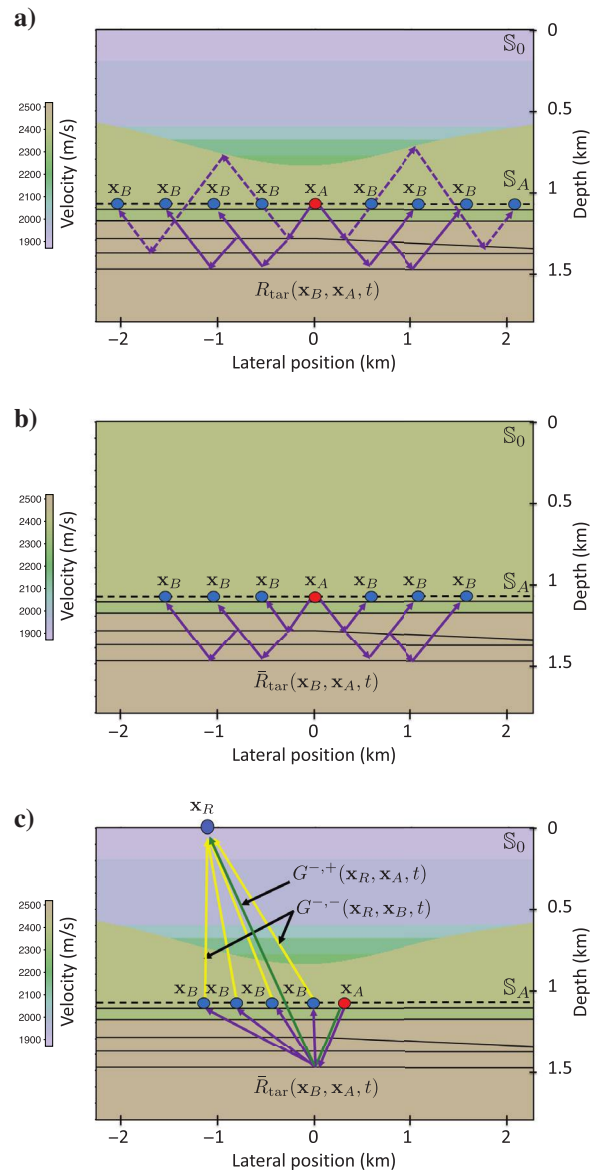


Figure 4. (a) The reflection response $R_{\text{tar}}(\mathbf{x}_B, \mathbf{x}_A, t) = G^{-,+}(\mathbf{x}_B, \mathbf{x}_A, t)$ in the actual medium. (b) The reflection response $\bar{R}_{\text{tar}}(\mathbf{x}_B, \mathbf{x}_A, t) = \bar{G}^{-,+}(\mathbf{x}_B, \mathbf{x}_A, t)$ in the truncated medium. (c) Visualization of equation 23. The Green's functions are shown in more detail in Figure 2a and the reflection response $\bar{R}_{\text{tar}}(\mathbf{x}_B, \mathbf{x}_A, t)$ in Figure 4b.

disadvantage compared to redatuming by MDD, which delivers the response $\bar{R}_{\text{tar}}(\mathbf{x}_B, \mathbf{x}_A, t)$ in the truncated medium (Figure 4b). However, the fact that redatuming by double focusing does not require inversion often outweighs this disadvantage.

In the compact operator notation, equation 26 becomes

$$R_{\text{tar}} = f_1^{+t} G_{R,A}^{-,+}, \quad (27)$$

where superscript t denotes operator transposition (the operator f_1^{+t} acts on the receiver coordinate instead of on the source coordinate). Combined with equation 21, this gives

$$R_{\text{tar}} = f_1^{+t} \Psi_b R f_1^+. \quad (28)$$

We call this source and receiver redatuming by double focusing. Note the similarity with the classic redatuming scheme (Berkhout, 1982; Berryhill, 1984; Berkhout and Wapenaar, 1993), which in compact operator notation reads

$$R_{\text{tar}} \approx f_{1,d}^{+t} R f_{1,d}^+. \quad (29)$$

Recall that $f_{1,d}^+$ is the direct contribution of focusing operator f_1^+ ; see Figure 1a and 1b. Hence, equation 29 only accounts for primary waves. Operator f_1^+ in equation 28, however, accounts for primaries and internal multiple reflections in the overburden (the region between \mathbb{S}_0 and \mathbb{S}_A).

Upon substitution of equation 16 into equation 28, we obtain

$$R_{\text{tar}} = f_{1,d}^{+t} \Psi_b R f_{1,d}^+ - (-f_{1,d}^{+t} \Psi_b R \Omega f_{1,d}^+) - (-\Omega f_{1,d}^+) \Psi_b R f_{1,d}^+ - (-\Omega f_{1,d}^+) \Psi_b R \Omega f_{1,d}^+ + \dots, \quad (30)$$

with $\Omega = \Theta_a R^* \Theta_b R$ (Staring et al., 2018). The first term on the right side stands for primary redatuming. Each of the subsequent terms in this expansion accounts for the prediction and subtraction of a specific order of internal multiple reflections. In theory, the scheme converges, so when the reflection response is accurately known there is no need to apply this subtraction adaptively. However, in practice, there will be imperfections in R . The expansion in

equation 30 opens the possibility of implementing the redatuming scheme in an adaptive way, by applying weighting factors or adaptive filters, which will make the Marchenko redatuming more robust (van der Neut et al., 2015c). We emphasize that an adaptive implementation is only needed to compensate for imperfections in the reflection response and for attenuation but not for limitations of the theory. Field data applications of this method (2D and 3D) are presented by Staring et al. (2018) and Staring and Wapenaar (2020).

Once the data have been redatumed, they can be used as the input for imaging of the target zone below the redatuming level \mathbb{S}_A . In principle, any migration scheme can be used for this. This will lead to an image of the target zone, free of artifacts related to internal multiples in the overburden. However, internal multiples related to the target and multiples between reflectors below and above \mathbb{S}_A may still lead to artifacts. In the field data applications mentioned previously, these multiples do not play a significant role. Nevertheless, there is a way to further reduce the effects of these remaining multiples. Instead of redatuming to a single depth level, redatuming can be carried out to multiple depth levels, followed by migration of the regions between these depth levels. Ultimately, redatuming can be carried out to all depth levels at which an image is required, followed by selecting the zero-offset component at the zero time of the redatumed data, that is, $R_{\text{tar}}(\mathbf{x}_B, \mathbf{x}_B, t = 0)$. This function, for all \mathbf{x}_B in the region of interest, forms an image $r_{\text{im}}(\mathbf{x}_B)$ of the local reflection coefficient, free of artifacts related to all multiple reflections. Because in the latter approach only the $t = 0$ component of R_{tar} is selected, it suffices to replace f_1^{+t} in equation 28 by $f_{1,d}^{+t}$ and to skip the window function Ψ_b . Hence, the imaging scheme thus becomes

$$r_{\text{im}} = (f_{1,d}^{+t} R f_{1,d}^+)_{\mathbf{x}_B=\mathbf{x}_A, t=0}, \quad (31)$$

where r_{im} stands for $r_{\text{im}}(\mathbf{x}_B)$.

Plane-wave redatuming

Taner (1976) and Schultz and Claerbout (1978) design a method to synthesize the reflection response to a plane wave at the surface. Rietveld et al. (1992) modify this approach to synthesize plane-wave sources in the subsurface. An advantage is that an image of a target zone can be obtained by migrating only a limited number of plane-wave responses (with different illumination angles) instead of a relatively large number of point-source responses. The approach of Rietveld et al. (1992) uses the primary transmission response of the overburden to synthesize the plane-wave sources; hence, internal multiples are not taken into account. Meles et al. (2018) propose to use the focusing functions obtained with the Marchenko method to synthesize virtual plane-wave sources in the subsurface. With this method, plane-wave responses are obtained that are free of artifacts related to the internal multiples of the overburden. Here, we briefly discuss this method.

We start by defining the 3D plane-wave focusing function $\tilde{f}_1^\pm(\mathbf{x}, \mathbf{p}_A, t)$ in the truncated medium (which is reflection-free below \mathbb{S}_A) as the integral of focusing functions $f_1^\pm(\mathbf{x}, \mathbf{x}_A, t)$ over all possible focal points \mathbf{x}_A at \mathbb{S}_A , according to

$$\tilde{f}_1^\pm(\mathbf{x}, \mathbf{p}_A, t) = \int_{\mathbb{S}_A} f_1^\pm(\mathbf{x}, \mathbf{x}_A, t - \mathbf{p} \cdot \mathbf{x}_{H,A}) d\mathbf{x}_A, \quad (32)$$

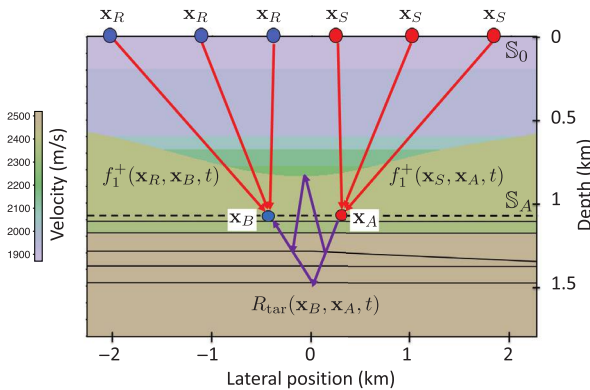


Figure 5. Visualization of equation 26 (receiver redatuming), applied to the output of equation 19 (source redatuming; see Figure 3b). The combination of these two processes (captured by equation 28) is called redatuming by double focusing. The red rays indicate the focusing function (shown in more detail in Figure 1a), and the purple rays represent the redatumed reflection response at \mathbb{S}_A in the actual medium (shown in more detail in Figure 4a).

with $\mathbf{p} = (p_1, p_2)$ and \mathbf{p}_A being a short notation for $(\mathbf{p}, x_{3,A})$. Here, p_1 and p_2 are the horizontal ray parameters. For a laterally constant velocity c at \mathbb{S}_A , the ray parameters are related to the dip angle α and the azimuth angle β via $p_1 = c^{-1} \sin \alpha \cos \beta$ and $p_2 = c^{-1} \sin \alpha \sin \beta$; for 2D situations, vector \mathbf{p} reduces to $\mathbf{p} = p_1$, with $p_1 = c^{-1} \sin \alpha$. The following derivation does not rely on a laterally constant velocity assumption.

When $\mathbf{p} = \mathbf{0}$, equation 32 integrates the focusing functions of Figure 1 without a time delay; hence, $\tilde{f}_1^+(\mathbf{x}, \mathbf{0}, x_{3,A}, t)$ focuses as a horizontal plane wave at \mathbb{S}_A and $t = 0$ and continues as a horizontal downgoing plane wave into the half-space below \mathbb{S}_A . For arbitrary \mathbf{p} , $\tilde{f}_1^+(\mathbf{x}, \mathbf{p}_A, t)$ focuses as a dipping plane wave at \mathbb{S}_A , according to

$$\tilde{f}_1^+(\mathbf{x}'_A, \mathbf{p}_A, t) = \delta(t - \mathbf{p} \cdot \mathbf{x}'_{H,A}), \quad (33)$$

for \mathbf{x}'_A at \mathbb{S}_A (which follows from substituting equation 2 into equation 32). Note that, whereas the original focusing functions focus in space and time (equation 2), the plane-wave focusing function focuses in time only (equation 33). The upgoing focusing function $\tilde{f}_1^-(\mathbf{x}_R, \mathbf{p}_A, t)$ is the response of the truncated medium to $\tilde{f}_1^+(\mathbf{x}_S, \mathbf{p}_A, t)$, observed at \mathbf{x}_R at \mathbb{S}_0 . The downgoing and upgoing plane-wave functions are visualized in Figure 6a.

We define the plane-wave Green's functions in the actual medium in a similar way; hence,

$$\tilde{G}^{-,\pm}(\mathbf{x}_R, \mathbf{p}_A, t) = \int_{\mathbb{S}_A} G^{-,\pm}(\mathbf{x}_R, \mathbf{x}_A, t - \mathbf{p} \cdot \mathbf{x}_{H,A}) d\mathbf{x}_A. \quad (34)$$

Here, $\tilde{G}^{-,+}(\mathbf{x}_R, \mathbf{p}_A, t)$ is interpreted as the response to a source for dipping downgoing plane waves at \mathbb{S}_A , observed by receivers for upgoing waves at \mathbf{x}_R at \mathbb{S}_0 ; see Figure 6b. Similarly, $\tilde{G}^{-,-}(\mathbf{x}_R, \mathbf{p}_A, t)$ is interpreted as the response to a source for dipping upgoing plane waves at \mathbb{S}_A ; see Figure 6c.

Applying similar integrations to the left and right sides of equations 4 and 5, we obtain

$$\begin{aligned} \tilde{G}^{-,+}(\mathbf{x}_R, \mathbf{p}_A, t) + \tilde{f}_1^-(\mathbf{x}_R, \mathbf{p}_A, t) \\ = \int_{\mathbb{S}_0} d\mathbf{x}_S \int_0^\infty R(\mathbf{x}_R, \mathbf{x}_S, t') \tilde{f}_1^+(\mathbf{x}_S, \mathbf{p}_A, t - t') dt' \end{aligned} \quad (35)$$

and

$$\begin{aligned} \tilde{G}^{-,-}(\mathbf{x}_R, \mathbf{p}'_A, -t) + \tilde{f}_1^+(\mathbf{x}_R, \mathbf{p}_A, t) \\ = \int_{\mathbb{S}_0} d\mathbf{x}_S \int_{-\infty}^0 R(\mathbf{x}_R, \mathbf{x}_S, -t') \tilde{f}_1^-(\mathbf{x}_S, \mathbf{p}_A, t - t') dt', \end{aligned} \quad (36)$$

where \mathbf{p}'_A stands for $(-\mathbf{p}, x_{3,A})$. Equation 35 can be interpreted in a similar way as equation 4. The right side quantifies the response of the actual medium to the downgoing focusing function

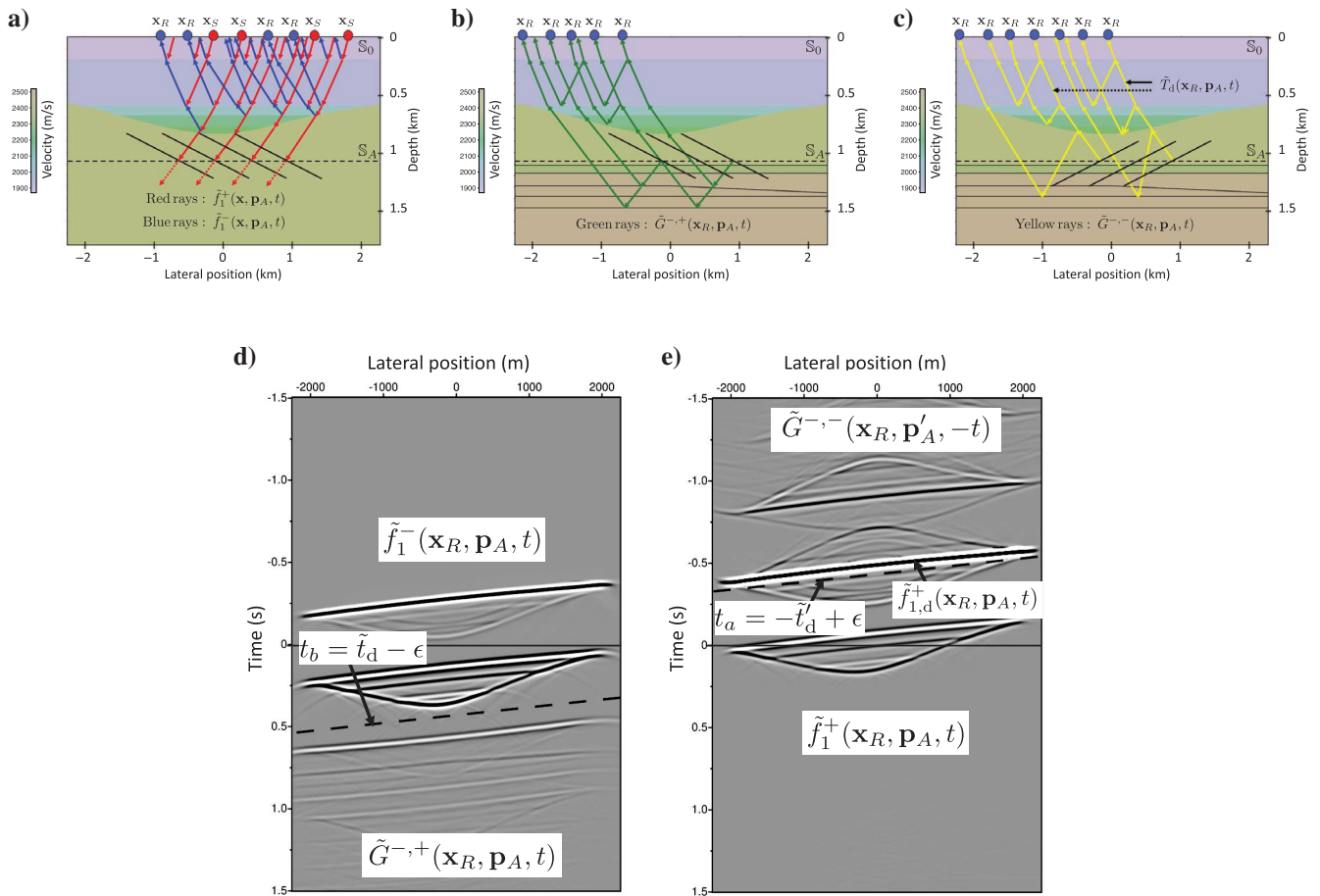


Figure 6. (a) Plane-wave focusing functions in the truncated medium (here shown for a negative value of p_1 and $p_2 = 0$). (b and c) Plane-wave Green's functions in the actual medium. (d) The left side of equation 35 (fixed \mathbf{p}_A , variable \mathbf{x}_R). (e) The left side of equation 36.

$\tilde{f}_1^+(\mathbf{x}_S, \mathbf{p}_A, t)$. In Figure 6a, it is seen that this gives the upgoing focusing function $\tilde{f}_1^-(\mathbf{x}_R, \mathbf{p}_A, t)$ at \mathbb{S}_0 and a focused plane wave at \mathbb{S}_A , which acts as a virtual source for downgoing plane waves. Figure 6b shows that the response to this virtual source is the Green's function $\tilde{G}^{-+}(\mathbf{x}_R, \mathbf{p}_A, t)$ on the left side of equation 35. Similarly, the right side of equation 36 quantifies the response of the time-reversed actual medium to the upgoing focusing function $\tilde{f}_1^-(\mathbf{x}_S, \mathbf{p}_A, t)$. The functions on the left sides of equations 35 and 36, convolved with a wavelet, are shown in gray-level display in Figure 6d and 6e, respectively.

To retrieve the plane-wave focusing functions from the reflection response R , we could first retrieve the functions $f_1^\pm(\mathbf{x}, \mathbf{x}_A, t)$ for all \mathbf{x}_A at \mathbb{S}_A and subsequently obtain $\tilde{f}_1^\pm(\mathbf{x}, \mathbf{p}_A, t)$ by evaluating equation 32. However, it is computationally much more efficient to retrieve these functions directly in the plane-wave domain, by suppressing the plane-wave Green's functions from equations 35 and 36 and solving the remaining system of equations for the plane-wave focusing functions. To determine the window functions for suppressing the Green's functions, we need to know the first possible arrival of $\tilde{G}^{-+}(\mathbf{x}_R, \mathbf{p}_A, t)$ and the last arrival of the time-reversed function $\tilde{G}^{-+}(\mathbf{x}_R, \mathbf{p}'_A, -t)$. The first possible arrival of $\tilde{G}^{-+}(\mathbf{x}_R, \mathbf{p}_A, t)$ (which would occur when there would be a reflector just below \mathbb{S}_A) is obtained by substituting equation 6 into equation 34; hence,

$$\{\tilde{G}^{-+}(\mathbf{x}_R, \mathbf{p}_A, t)\}''_{\text{first}} \propto \int_{\mathbb{S}_A} T_d(\mathbf{x}_R, \mathbf{x}_A, t - \mathbf{p} \cdot \mathbf{x}_{H,A}) d\mathbf{x}_A = \tilde{T}_d(\mathbf{x}_R, \mathbf{p}_A, t). \quad (37)$$

Here, $\tilde{T}_d(\mathbf{x}_R, \mathbf{p}_A, t)$ is the direct arrival of the transmission response to a dipping plane wave, emitted upward from \mathbb{S}_A with ray parameter \mathbf{p} , observed by a receiver at \mathbf{x}_R (this is also the direct arrival of $\tilde{G}^{-+}(\mathbf{x}_R, \mathbf{p}_A, t)$; see Figure 6c). We denote the arrival time of this direct transmission response as $\tilde{t}_d(\mathbf{x}_R, \mathbf{p}_A)$. Hence, $\tilde{G}^{-+}(\mathbf{x}_R, \mathbf{p}_A, t)$ can be suppressed from equation 35 by a time window that removes everything beyond $t = t_b = \tilde{t}_d(\mathbf{x}_R, \mathbf{p}_A) - \epsilon$ (the dashed line in Figure 6d, indicated by $t_b = \tilde{t}_d - \epsilon$). The last arrival of the time-reversed Green's function $\tilde{G}^{-+}(\mathbf{x}_R, \mathbf{p}'_A, -t)$ is obtained by substituting equation 7 into equation 34; hence

$$\{\tilde{G}^{-+}(\mathbf{x}_R, \mathbf{p}'_A, -t)\}_{\text{last}} = -\tilde{T}_d(\mathbf{x}_R, \mathbf{p}'_A, -t). \quad (38)$$

The arrival time of this event is $-\tilde{t}_d(\mathbf{x}_R, \mathbf{p}'_A)$. Hence, $\tilde{G}^{-+}(\mathbf{x}_R, \mathbf{p}'_A, -t)$ can be suppressed from equation 36 by a time window that removes everything before $t = t_a = -\tilde{t}_d(\mathbf{x}_R, \mathbf{p}'_A) + \epsilon$ (the dashed line in Figure 6e, indicated by $t_a = -\tilde{t}'_d + \epsilon$). We define two time windows as

$$\tilde{\Theta}_a(\mathbf{x}_R, \mathbf{p}_A, t) = \theta(t - t_a) = \theta(t + \tilde{t}'_d - \epsilon), \quad (39)$$

$$\tilde{\Theta}_b(\mathbf{x}_R, \mathbf{p}_A, t) = \theta(t_b - t) = \theta(\tilde{t}_d - \epsilon - t). \quad (40)$$

These windows suppress the Green's functions and pass the focusing functions f_1^+ and \tilde{f}_1^- , except the direct plane-wave arrival $\tilde{f}_{1,d}^+(\mathbf{x}_R, \mathbf{p}_A, t)$, which coincides with the last arrival of $\tilde{G}^{-+}(\mathbf{x}_R, \mathbf{p}'_A, -t)$; see Figure 6e.

Application of the windows $\tilde{\Theta}_{a,b}(\mathbf{x}_R, \mathbf{p}_A, t)$ to both sides of equations 35 and 36 gives, in compact operator notation,

$$\tilde{f}_1^- = \tilde{\Theta}_b R \tilde{f}_1^+, \quad (41)$$

$$\tilde{f}_1^+ = \tilde{\Theta}_a R^* \tilde{f}_1^- + \tilde{f}_{1,d}^+. \quad (42)$$

These are the Marchenko equations for the plane-wave focusing functions. They can be solved, analogous to equation 16, by

$$\tilde{f}_1^+ = \sum_{k=0}^K \{\tilde{\Theta}_a R^* \tilde{\Theta}_b R\}^k \tilde{f}_{1,d}^+. \quad (43)$$

The next step is the retrieval of the plane-wave Green's functions. We define complementary time windows as $\tilde{\Psi}_{a,b}(\mathbf{x}_R, \mathbf{p}_A, t) = 1 - \tilde{\Theta}_{a,b}(\mathbf{x}_R, \mathbf{p}_A, t)$. Application of these windows to both sides of equations 35 and 36 gives, in compact operator notation,

$$\tilde{G}_{R,\mathbf{p}_A}^{-,+} = \tilde{\Psi}_b R \tilde{f}_1^+, \quad (44)$$

$$\tilde{G}_{R,\mathbf{p}'_A}^{-,*} = \tilde{\Psi}_a R^* \tilde{f}_1^- - \tilde{f}_{1,d}^+, \quad (45)$$

where the subscripts on the left sides refer to the position of the actual receiver and the ray parameter of the virtual plane-wave source.

The interpretation of equations 44 and 45 is that they accomplish source redatuming from \mathbf{x}_S at the acquisition surface \mathbb{S}_0 to a virtual plane-wave source at the datum plane \mathbb{S}_A in the subsurface. Figure 7a visualizes equation 44.

Analogous to equations 27 and 28, the receivers can now be redatumed from \mathbf{x}_R at the surface \mathbb{S}_0 to a virtual receiver at \mathbf{x}_B at \mathbb{S}_A , according to

$$\tilde{R}_{\text{tar}} = f_1^{+t} \tilde{G}_{R,\mathbf{p}_A}^{-,+} = f_1^{+t} \tilde{\Psi}_b R \tilde{f}_1^+, \quad (46)$$

where \tilde{R}_{tar} stands for the target reflection response $\tilde{R}_{\text{tar}}(\mathbf{x}_B, \mathbf{p}_A, t) = G^{-+}(\mathbf{x}_B, \mathbf{p}_A, t)$; see Figure 7b. It is the response to a virtual downgoing plane-wave source at \mathbb{S}_A with ray parameter \mathbf{p} , observed by a virtual receiver for upgoing waves at \mathbf{x}_B . Note that the Marchenko method needs to be applied for each virtual receiver of interest. Hence, the computational advantage of plane-wave source-redatuming, which is typically limited to a small number of ray parameters, quickly diminishes when many virtual receiver positions are chosen. However, if we combine redatuming with imaging, we can replace the focusing function f_1^{+t} by its direct arrival $f_{1,d}^{+t}$ and skip the window function $\tilde{\Psi}_b$, similar to the procedure in imaging by double focusing (equation 31); hence,

$$\tilde{r}_{\text{im}} = (f_{1,d}^{+t} R \tilde{f}_1^+)_{t=\mathbf{p} \cdot \mathbf{x}_{H,B}}, \quad (47)$$

where \tilde{r}_{im} stands for the angle-dependent local reflection coefficient $\tilde{r}_{\text{im}}(\mathbf{x}_B, \mathbf{p}_A)$ for all \mathbf{x}_B in the region of interest. Note that the imaging condition $t = \mathbf{p} \cdot \mathbf{x}_{H,B}$ (instead of $t = 0$) accounts for the fact that the virtual plane-wave source at depth $x_{3,A}$ is dipping when $\mathbf{p} \neq \mathbf{0}$. Using equation 47 as the basis for redatuming and imaging, the Marchenko method is only needed to retrieve the plane-wave focusing function \tilde{f}_1^+ for a limited number of ray parameters at each imaging depth. This implies a significant efficiency gain in comparison with redatuming and imaging based on equation 31, particularly for 3D applications. Meles et al. (2018) discuss applications of plane-wave redatuming and imaging to 2D numerically modeled data.

MARCHENKO MULTIPLE ELIMINATION

All redatuming methods discussed in the ‘‘Marchenko redatuming and imaging’’ section have in common that internal multiples are eliminated between the surface and the virtual sources and/or receivers in the subsurface. The required input for these methods consists of the reflection response at the surface (after surface-related-multiple elimination and deconvolution for the wavelet) and the direct arrivals of the focusing functions. The latter can be derived, for example, from a macro velocity model of the subsurface.

Meles et al. (2016) propose to extrapolate the virtual receivers (or, equivalently, the virtual sources) upward to the acquisition surface, using direct-wave Green’s functions. The result is a reflection response with sources and receivers at the surface, from which part of the internal multiples are eliminated. Because the direct-wave Green’s functions are defined in the same velocity model as the direct arrivals of the focusing functions, the combined process of focusing and upward extrapolation is significantly less sensitive to errors in the velocity model than the focusing as a stand-alone process.

Building on this idea, several Marchenko-based methods have been developed that extrapolate the virtual sources and receivers to the surface. However, instead of applying the extrapolation after Marchenko redatuming, in these methods the extrapolation operator is integrated in the Marchenko method. Because these methods yield reflection data at the surface with fewer internal multiples (van der Neut and Wapenaar, 2016), or even without any internal multiples (Zhang et al., 2019b), we refer to these methods as ‘‘Marchenko multiple elimination’’ (as opposed to ‘‘Marchenko redatuming,’’ which yields reflection data with fewer internal multiples at a datum plane in the subsurface).

Marchenko multiple elimination operates in the same domain as other internal multiple elimination methods in the literature (Berkhout and Verschuur, 1997; Weglein et al., 1997, 2003; Jakubowicz, 1998; ten Kroode, 2002; van Borselen, 2002; Verschuur and Berkhout, 2005; Ikelle, 2006). A comparison with these methods is beyond the scope of this paper. A specific characteristic of Marchenko multiple elimination is that it predicts and subtracts all orders of internal multiples with correct amplitudes. In the following, we discuss Marchenko multiple elimination methods step-by-step.

Representations, extrapolated to the surface

We use the direct arrival of the transmission response of the truncated medium, $T_d(\mathbf{x}_A, \mathbf{x}_S, t)$, as an operator to extrapolate wavefield quantities from \mathbb{S}_A in the subsurface to the acquisition surface \mathbb{S}_0 . According to equation 17, the direct arrivals of the transmission response and of the focusing function are each other’s (band-limited) inverse. Here, we reformulate equation 17 in terms of an integral along \mathbb{S}_A , as follows:

$$\delta(\mathbf{x}_{H,R} - \mathbf{x}'_{H,S})\delta(t) = \int_{\mathbb{S}_A} d\mathbf{x}_A \int_{-\infty}^t f_{1,d}^+(\mathbf{x}_R, \mathbf{x}_A, t') T_d(\mathbf{x}_A, \mathbf{x}'_S, t - t') dt', \tag{48}$$

with \mathbf{x}_R and \mathbf{x}'_S at \mathbb{S}_0 . We use the operation $\int_{\mathbb{S}_A} d\mathbf{x}_A \int_{-\infty}^t \{\cdot\} T_d(\mathbf{x}_A, \mathbf{x}'_S, t - t') dt'$ to define the extrapolated focusing functions and Green’s functions as

$$v^\pm(\mathbf{x}_R, \mathbf{x}'_S, t; x_{3,A}) = \int_{\mathbb{S}_A} d\mathbf{x}_A \int_{-\infty}^t f_1^\pm(\mathbf{x}_R, \mathbf{x}_A, t') T_d(\mathbf{x}_A, \mathbf{x}'_S, t - t') dt' \tag{49}$$

and

$$U^{-,\pm}(\mathbf{x}_R, \mathbf{x}'_S, \pm t; x_{3,A}) = \int_{\mathbb{S}_A} d\mathbf{x}_A \int_{-\infty}^t G^{-,\pm}(\mathbf{x}_R, \mathbf{x}_A, \pm t') T_d(\mathbf{x}_A, \mathbf{x}'_S, t - t') dt', \tag{50}$$

respectively (van der Neut and Wapenaar, 2016). Equation 50 for $U^{-,+}(\mathbf{x}_R, \mathbf{x}'_S, t; x_{3,A})$ describes the extrapolation of the source of $G^{-,+}(\mathbf{x}_R, \mathbf{x}_A, t)$ from \mathbf{x}_A at \mathbb{S}_A to \mathbf{x}'_S at the surface \mathbb{S}_0 . The resulting response $U^{-,+}(\mathbf{x}_R, \mathbf{x}'_S, t; x_{3,A})$ can be interpreted as the reflection response between \mathbf{x}'_S and \mathbf{x}_R at the surface \mathbb{S}_0 , in which the wavefield between the source at \mathbf{x}'_S and \mathbb{S}_A (at depth $x_{3,A}$) consists of the direct downgoing wave only. This is visualized in Figure 8.

Applying the same extrapolation operation to the left and right sides of equations 4 and 5, we obtain

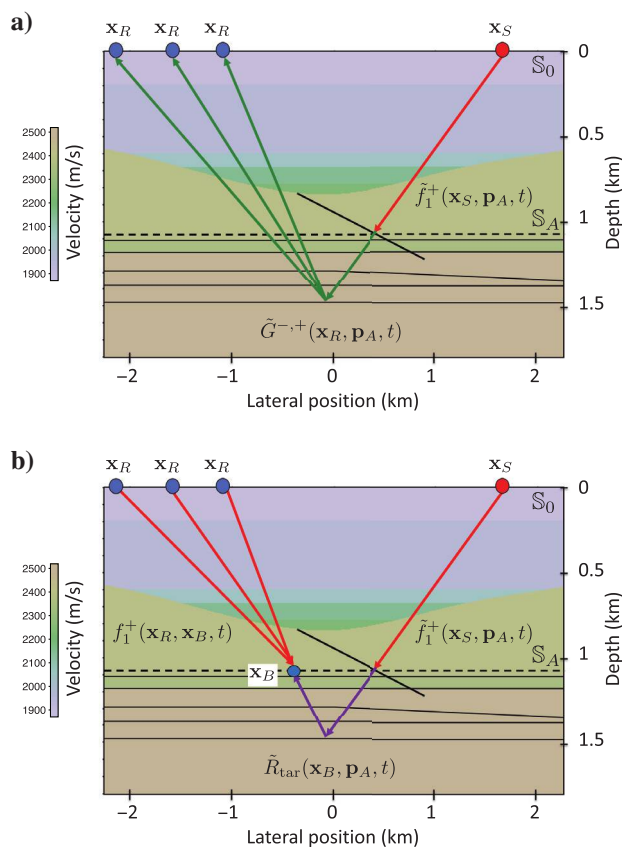


Figure 7. (a) Visualization of equation 44 (plane-wave source redatuming). The red ray indicates the plane-wave focusing function (shown in more detail in Figure 6a) and the green rays represent the plane-wave Green’s function (shown in more detail in Figure 6b). (b) Visualization of equation 46. The focusing function $\tilde{f}_1^+(\mathbf{x}_R, \mathbf{x}_B, t)$ is shown in more detail in Figure 1a. The purple rays represent the redatumed plane-wave reflection response at \mathbb{S}_A in the actual medium.

$$U^{-,+}(\mathbf{x}_R, \mathbf{x}'_S, t; x_{3,A}) + v^{-}(\mathbf{x}_R, \mathbf{x}'_S, t; x_{3,A}) = \int_{\mathbb{S}_0} d\mathbf{x}_S \int_0^\infty R(\mathbf{x}_R, \mathbf{x}_S, t') v^+(\mathbf{x}_S, \mathbf{x}'_S, t - t'; x_{3,A}) dt' \quad (51)$$

and

$$U^{-,-}(\mathbf{x}_R, \mathbf{x}'_S, -t; x_{3,A}) + v^+(\mathbf{x}_R, \mathbf{x}'_S, t; x_{3,A}) = \int_{\mathbb{S}_0} d\mathbf{x}_S \int_{-\infty}^0 R(\mathbf{x}_R, \mathbf{x}_S, -t') v^-(\mathbf{x}_S, \mathbf{x}'_S, t - t'; x_{3,A}) dt'. \quad (52)$$

The functions on the left sides of equations 51 and 52, convolved with a wavelet, are shown in gray-level display in Figure 9a and 9b, respectively.

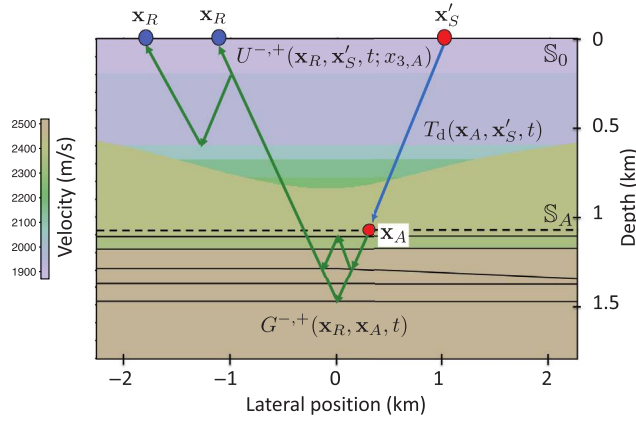


Figure 8. Visualization of equation 50 (extrapolation of the source from \mathbf{x}_A at \mathbb{S}_A to \mathbf{x}'_S at the surface \mathbb{S}_0).

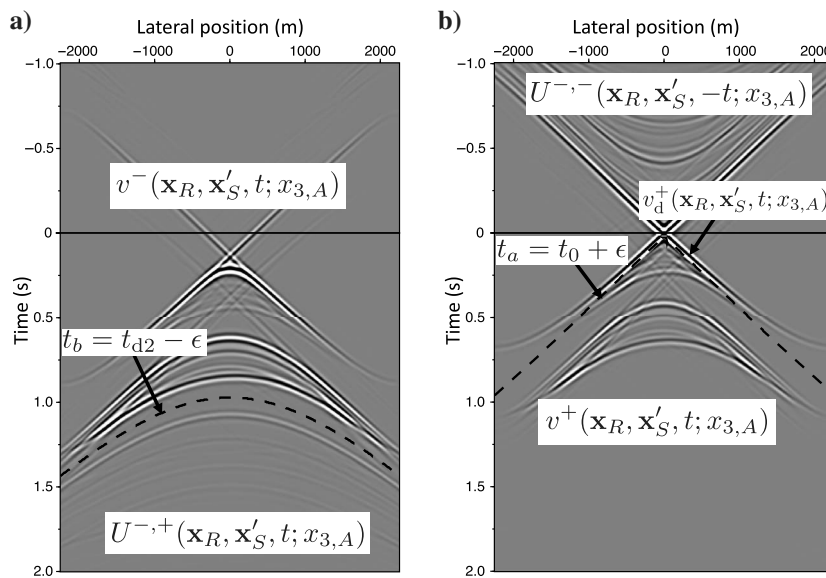


Figure 9. (a) The left side of equation 51 (fixed \mathbf{x}'_S , variable \mathbf{x}_R). (b) The left side of equation 52.

Retrieval of extrapolated focusing functions

To determine the window functions for suppressing the extrapolated Green's functions from equations 51 and 52, we need to know the first possible arrival of $U^{-,+}(\mathbf{x}_R, \mathbf{x}'_S, t; x_{3,A})$ and the last arrival of the time-reversed function $U^{-,-}(\mathbf{x}_R, \mathbf{x}'_S, -t; x_{3,A})$. The first possible arrival of $U^{-,+}(\mathbf{x}_R, \mathbf{x}'_S, t; x_{3,A})$ (which would occur when there would be a reflector just below \mathbb{S}_A) is obtained by substituting equation 6 into equation 50; hence,

$$\{U^{-,+}(\mathbf{x}_R, \mathbf{x}'_S, t; x_{3,A})\}_{\text{first}} \propto \int_{\mathbb{S}_A} d\mathbf{x}_A \int_0^t T_d(\mathbf{x}_R, \mathbf{x}_A, t') T_d(\mathbf{x}_A, \mathbf{x}'_S, t - t') dt'. \quad (53)$$

Note that T_d is convolved with itself and integrated along \mathbb{S}_A . The main contribution comes from the stationary point on \mathbb{S}_A , which corresponds to the specular reflection point; see Figure 10a. Hence, this integral yields the direct arrival of the reflection response of the hypothetical reflector just below \mathbb{S}_A . The arrival time of this event is the two-way traveltimes $t_{d2}(\mathbf{x}_R, \mathbf{x}'_S; x_{3,A})$. Hence, $U^{-,+}(\mathbf{x}_R, \mathbf{x}'_S, t; x_{3,A})$ can be suppressed from equation 51 by a time window that removes everything beyond $t = t_b = t_{d2}(\mathbf{x}_R, \mathbf{x}'_S; x_{3,A}) - \epsilon$ (the dashed line in Figure 9a). The last arrival of $U^{-,-}(\mathbf{x}_R, \mathbf{x}'_S, -t; x_{3,A})$ is obtained by substituting equation 7 into equation 50; hence,

$$\{U^{-,-}(\mathbf{x}_R, \mathbf{x}'_S, -t; x_{3,A})\}_{\text{last}} = - \int_{\mathbb{S}_A} d\mathbf{x}_A \int_{-\infty}^0 T_d(\mathbf{x}_R, \mathbf{x}_A, -t') T_d(\mathbf{x}_A, \mathbf{x}'_S, t - t') dt'. \quad (54)$$

As opposed to equation 53, here T_d is correlated with itself and integrated along \mathbb{S}_A ; see Figure 10b. Hence, this integral yields a band-limited focus around $\mathbf{x}_R = \mathbf{x}'_S$ and $t = 0$. We denote the traveltimes curve of this focus at positive time as $t_0(\mathbf{x}_R, \mathbf{x}'_S)$. This is zero for zero offset (i.e., $t_0(\mathbf{x}'_S, \mathbf{x}'_S) = 0$) and increases linearly with the increasing offset between \mathbf{x}'_S and \mathbf{x}_R . Hence, $U^{-,-}(\mathbf{x}_R, \mathbf{x}'_S, -t; x_{3,A})$ can be suppressed from equation 52 by a time window that removes everything before $t = t_a = t_0(\mathbf{x}_R, \mathbf{x}'_S) + \epsilon$ (the dashed line in Figure 9b). We define two time windows as

$$\Theta_a^v(\mathbf{x}_R, \mathbf{x}'_S, t; x_{3,A}) = \theta(t - t_a) = \theta(t - t_0 - \epsilon), \quad (55)$$

$$\Theta_b^v(\mathbf{x}_R, \mathbf{x}'_S, t; x_{3,A}) = \theta(t_b - t) = \theta(t_{d2} - \epsilon - t). \quad (56)$$

These windows suppress the extrapolated Green's functions and pass the extrapolated focusing functions v^+ and v^- (hence, the superscript v in $\Theta_{a,b}^v$), except the extrapolated direct arrival $v_d^+(\mathbf{x}_R, \mathbf{x}'_S, t; x_{3,A})$, which coincides with the last arrival of $U^{-,-}(\mathbf{x}_R, \mathbf{x}'_S, -t; x_{3,A})$; see Figure 9b. This extrapolated direct arrival is, analogous to equation 49, defined as

$$v_d^+(\mathbf{x}_R, \mathbf{x}'_S, t; x_{3,A}) = \int_{\mathbb{S}_A} d\mathbf{x}_A \int_{-\infty}^t f_{1,d}^+(\mathbf{x}_R, \mathbf{x}_A, t') T_d(\mathbf{x}_A, \mathbf{x}'_S, t-t') dt', \quad (57)$$

or, using equation 48,

$$v_d^+(\mathbf{x}_R, \mathbf{x}'_S, t; x_{3,A}) = \delta(\mathbf{x}_{H,R} - \mathbf{x}'_{H,S}) \delta(t), \quad (58)$$

where the delta functions should be interpreted again in a band-limited sense.

Application of the windows $\Theta_{a,b}^v(\mathbf{x}_R, \mathbf{x}'_S, t; x_{3,A})$ to both sides of equations 51 and 52 gives, in the compact operator notation,

$$v^- = \Theta_b^v R v^+, \quad (59)$$

$$v^+ = \Theta_a^v R^* v^- + v_d^+, \quad (60)$$

with $v_d^+ = \delta$; see equation 58. These are the Marchenko equations for the extrapolated focusing functions. They can be solved, analogous to equation 16, by

$$v^+ = \sum_{k=0}^K \{\Theta_a^v R^* \Theta_b^v R\}^k \delta. \quad (61)$$

An important difference with equation 16 is that equation 61 does not contain the direct arrival of the focusing function, $f_{1,d}^+$. Instead, it contains the delta function, which, according to equation 58, depends only on the lateral source position $\mathbf{x}'_{H,S}$ but not on a model of the medium. This is a significant advantage of the Marchenko scheme of equation 61 over that of equation 16. Note that the window function Θ_b^v contains the two-way traveltime $t_{d2}(\mathbf{x}_R, \mathbf{x}'_S; x_{3,A})$ and hence implicitly depends on the medium. However, according to our experience, errors in the window functions have much less effect on the retrieved focusing functions than errors in the estimated direct arrival $f_{1,d}^+$ in equation 16.

Similar assumptions as discussed following equation 9 apply for the retrieval of the extrapolated focusing functions. [Elison et al. \(2020\)](#) discuss how to account for thin layering, assuming that the medium between \mathbb{S}_0 and \mathbb{S}_A is horizontally layered.

Retrieval of extrapolated Green's functions (source-side dereverberation)

The next step is the retrieval of the extrapolated Green's functions. We define the complementary time windows as

$$\Psi_{a,b}^v(\mathbf{x}_R, \mathbf{x}'_S, t; x_{3,A}) = 1 - \Theta_{a,b}^v(\mathbf{x}_R, \mathbf{x}'_S, t; x_{3,A}). \quad (62)$$

Application of these windows to both sides of equations 51 and 52 gives, in the compact operator notation,

$$U_{R,S'}^{-,+} = \Psi_b^v R v^+, \quad (63)$$

$$U_{R,S'}^{-,*} = \Psi_a^v R^* v^- - v_d^+, \quad (64)$$

where the subscripts on the left sides refer to the position of the actual receiver and the extrapolated virtual source, both at \mathbb{S}_0 .

We interpret equation 63 as follows. The extrapolated focusing function v^+ is applied to the reflection response R at the surface \mathbb{S}_0 . The result is $U_{R,S'}^{-,+}$, which is the reflection response at the surface \mathbb{S}_0 ,

in which the wavefield between the source at \mathbf{x}'_S and \mathbb{S}_A consists of the direct downgoing wave only (Figure 8). Because the multiples in the downgoing wavefield are removed, we refer to the process described by equation 63 as dereverberation at the source side. Hence, where applicable, we call the extrapolated focusing function v^+ a dereverberation operator.

Before we discuss dereverberation at the receiver side, we spend some more words on equation 63. Substitution of equation 61 for v^+ yields

$$U_{R,S'}^{-,+} = \Psi_b^v [R - (-R\Theta_a^v R^* \Theta_b^v R) - (-R\Theta_a^v R^* \Theta_b^v R \Theta_a^v R^* \Theta_b^v R) \cdots]. \quad (65)$$

The first term between the square brackets is the reflection response. The subsequent terms predict internal multiples, which are subtracted from the reflection response. Note that the internal multiples are predicted via correlations and convolutions of the reflection response with itself. [Jakubowicz \(1998\)](#) introduces the prediction of first-order internal multiples as (in our notation) $-RR^*R$, where specific events have to be selected in the different versions of R in this expression. Hence, equation 65 or, more generally, equation 63 with v^+ defined in equation 61, can be seen as a generalization of the method proposed by [Jakubowicz \(1998\)](#), for predicting and

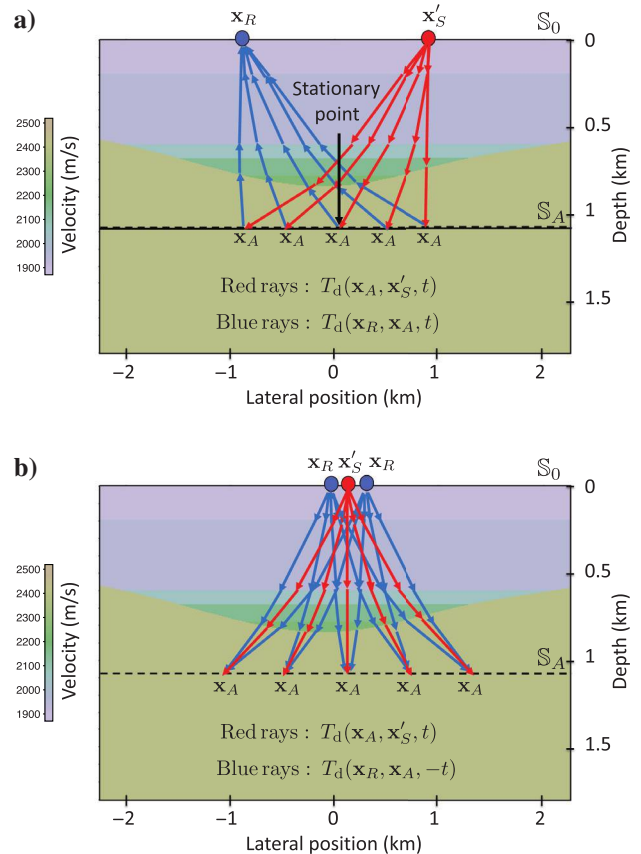


Figure 10. (a) Visualization of equation 53. Convolution of the transmission responses yields a reflection response (the ray via the stationary point). (b) Visualization of equation 54. Correlation of the transmission responses yields a band-limited focus around \mathbf{x}'_S .

subtracting all orders of internal multiple reflections on the source side between \mathbb{S}_0 and \mathbb{S}_A . The window functions $\Theta_{a,b}^v$ and Ψ_b^v , defined in equations 55, 56, and 62, take care of the proper selection of the events that take part in the multiple prediction. In the following, we discuss different methods to predict and subtract also the internal multiples on the receiver side.

Receiver-side dereverberation by MDD

Analogous to equation 23, which underlies redatuming by MDD, we formulate the following relation between the extrapolated Green's functions:

$$U_{R,S'}^{-,+}(\mathbf{x}_R, \mathbf{x}'_S, t) = - \int_{\mathbb{S}_0} d\mathbf{x}'_R \int_0^t U_{R,R'}^{-,-}(\mathbf{x}_R, \mathbf{x}'_R, t') \bar{R}_{\text{ddr}}^{\text{trc}}(\mathbf{x}'_R, \mathbf{x}'_S, t-t'; x_{3,A}) dt'. \quad (66)$$

Whereas equation 23 is derived from wave theory, with $\bar{R}_{\text{tar}}(\mathbf{x}_B, \mathbf{x}_A, t)$ being the target reflection response of the truncated medium (Figure 4b), equation 66 is introduced purely based on analogy with equation 23. Hence, the physical meaning of $\bar{R}_{\text{ddr}}^{\text{trc}}(\mathbf{x}'_R, \mathbf{x}'_S, t; x_{3,A})$ still needs to be derived and the sub- and superscripts will be explained later. We start by rewriting equation 66 in the compact operator notation, as follows:

$$U_{R,S'}^{-,+} = -U_{R,R'}^{-,-} \bar{R}_{\text{ddr}}^{\text{trc}}. \quad (67)$$

Upon substitution of equation 50, we obtain

$$G_{R,A}^{-,+} T_d = -G_{R,B}^{-,-} T_d^* \bar{R}_{\text{ddr}}^{\text{trc}}, \quad (68)$$

hence,

$$\bar{R}_{\text{ddr}}^{\text{trc}} = -(T_d^*)^{-1} (G_{R,B}^{-,-})^{-1} G_{R,A}^{-,+} T_d. \quad (69)$$

On the right side, we recognize $-(G_{R,B}^{-,-})^{-1} G_{R,A}^{-,+}$ as the redatuming-by-MDD algorithm of equation 25, which gives \bar{R}_{tar} ; hence,

$$\bar{R}_{\text{ddr}}^{\text{trc}} = (T_d^*)^{-1} \bar{R}_{\text{tar}} T_d. \quad (70)$$

Note that $(T_d^*)^{-1}$ is the inverse of the time-reversed direct arrival of the transmission response of the medium between \mathbb{S}_0 and \mathbb{S}_A (where the inverse is understood in the sense of integral equation 48; hence, $(T_d^*)^{-1} = f_{1,d}^{+,*}$). Note that $(T_d^*)^{-1}$ has the same traveltimes as T_d , but different amplitudes. Whereas T_d includes transmission losses of the interfaces between \mathbb{S}_0 and \mathbb{S}_A , $(T_d^*)^{-1}$ compensates for such transmission losses. For the interpretation of equation 70, we refer to Figure 11a, which shows that $\bar{R}_{\text{ddr}}^{\text{trc}}(\mathbf{x}'_R, \mathbf{x}'_S, t; x_{3,A})$ can be seen as the reflection response between \mathbf{x}'_S and \mathbf{x}'_R at the surface \mathbb{S}_0 , in which the wavefields between \mathbb{S}_0 and \mathbb{S}_A consist of direct downgoing and upgoing waves only, and the response \bar{R}_{tar} at \mathbb{S}_A includes primaries and multiples of the target below \mathbb{S}_A (Figure 4b). Hence, $\bar{R}_{\text{ddr}}^{\text{trc}}$ is the reflection response at \mathbb{S}_0 , double-dereverberated at the source and receiver sides (denoted by the subscript “ddr”), and compensated for transmission losses in the medium between \mathbb{S}_0 and \mathbb{S}_A (denoted by superscript “trc”). The transmission-loss compensation would be exact when T_d and $(T_d^*)^{-1}$ would see the same interfaces, which is the case in horizontally layered media (Elison

et al., 2020); in laterally varying media, the transmission-loss compensation is approximate.

Next, we derive the algorithm for retrieving $\bar{R}_{\text{ddr}}^{\text{trc}}$ from the reflection response R . From equation 67, we obtain

$$\bar{R}_{\text{ddr}}^{\text{trc}} = -(U_{R,R'}^{-,-})^{-1} U_{R,S'}^{-,+}, \quad (71)$$

with $U_{R,S'}^{-,+}$ and $U_{R,R'}^{-,-}$ retrieved from equations 63 and 64. Equation 71 accomplishes receiver-side dereverberation by MDD. The algorithm is similar to receiver redatuming by MDD (equation 25), but it is significantly less sensitive to a model of the medium; see the discussion following equation 61. This is also explained by the fact that the sources and receivers of the input data $R(\mathbf{x}_R, \mathbf{x}_S, t)$ stay at the surface \mathbb{S}_0 in the output data $\bar{R}_{\text{ddr}}^{\text{trc}}(\mathbf{x}'_R, \mathbf{x}'_S, t; x_{3,A})$, instead of being redatumed to \mathbb{S}_A as in $\bar{R}_{\text{tar}}(\mathbf{x}_B, \mathbf{x}_A, t)$. A numerical example is shown by van der Neut and Wapenaar (2016). Dukalski and de Vos (2020) solve equation 67 for $\bar{R}_{\text{ddr}}^{\text{trc}}$ with an easier-than-MDD inversion. In the next section, we derive an alternative double-dereverberation method, which also avoids the MDD process.

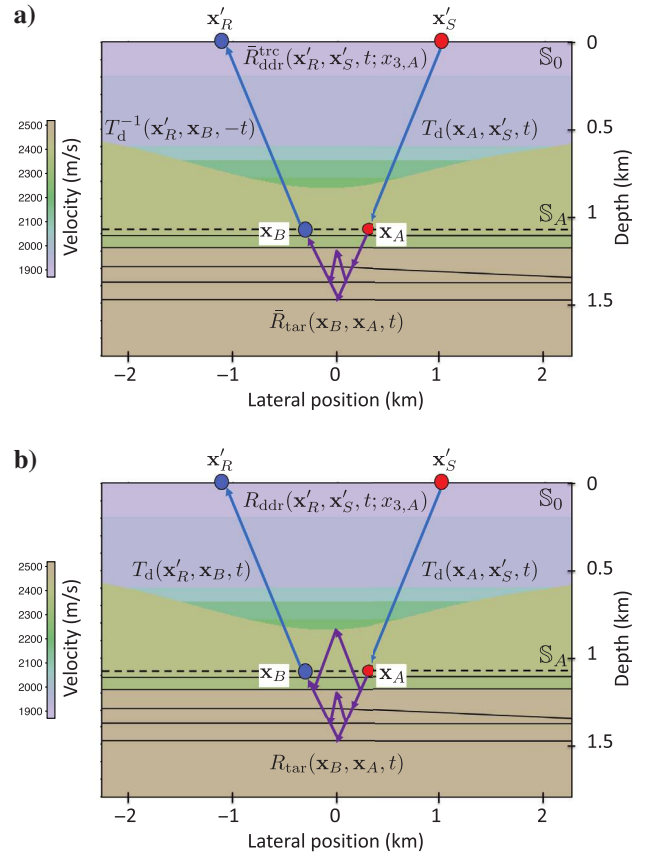


Figure 11. (a) Visualization of equation 70. The purple rays represent the target reflection response at \mathbb{S}_A in the truncated medium (shown in more detail in Figure 4b). (b) Visualization of equation 76. The purple rays represent the target reflection response at \mathbb{S}_A in the actual medium (shown in more detail in Figure 4a).

Source- and receiver-side dereverberation by double extrapolated focusing

Analogous to equation 26, which formulates receiver redatuming, we apply the dereverberation operator $v^+(\mathbf{x}_R, \mathbf{x}'_R, t; x_{3,A})$ to the receiver side of the extrapolated Green's function $U^{-,+}(\mathbf{x}_R, \mathbf{x}'_S, t; x_{3,A})$, according to

$$R_{\text{ddr}}(\mathbf{x}'_R, \mathbf{x}'_S, t; x_{3,A}) = \int_{\mathbb{S}_0} d\mathbf{x}_R \int_0^\infty v^+(\mathbf{x}_R, \mathbf{x}'_R, t-t'; x_{3,A}) U^{-,+}(\mathbf{x}_R, \mathbf{x}'_S, t'; x_{3,A}) dt' \quad (72)$$

(Dukalski and de Vos, 2020; Reinicke and Dukalski, 2020; Staring et al., 2021). To derive the physical meaning of $R_{\text{ddr}}(\mathbf{x}'_R, \mathbf{x}'_S, t; x_{3,A})$ on the left side, we analyze the right side step by step. In the compact operator notation, equation 72 becomes

$$R_{\text{ddr}} = v^{+,+} U_{R,S'}^{-,+} \quad (73)$$

Upon substitution of equations 49 and 50 into equation 73, we obtain

$$R_{\text{ddr}} = T_d^t f_1^{+,+} G_{R,A}^{-,+} T_d \quad (74)$$

or, upon substitution of equation 21,

$$R_{\text{ddr}} = T_d^t f_1^{+,+} (\Psi_b R f_1^+) T_d \quad (75)$$

On the right side, we recognize $f_1^{+,+} \Psi_b R f_1^+$ as the redatuming by double-focusing algorithm of equation 28, which gives R_{tar} ; hence,

$$R_{\text{ddr}} = T_d^t R_{\text{tar}} T_d \quad (76)$$

This equation describes the extrapolation of the source and receiver of $R_{\text{tar}}(\mathbf{x}_B, \mathbf{x}_A, t)$ from \mathbb{S}_A to the surface \mathbb{S}_0 , yielding $R_{\text{ddr}}(\mathbf{x}'_R, \mathbf{x}'_S, t; x_{3,A})$; see Figure 11b. The term $R_{\text{ddr}}(\mathbf{x}'_R, \mathbf{x}'_S, t; x_{3,A})$ is interpreted as the reflection response between \mathbf{x}'_S and \mathbf{x}'_R at the surface \mathbb{S}_0 , in which the wavefields between \mathbb{S}_0 and \mathbb{S}_A consist of the direct downgoing and upgoing waves only and the response R_{tar} at \mathbb{S}_A includes primaries and multiples of the target below \mathbb{S}_A (and multiples between reflectors below and above \mathbb{S}_A , Figure 4a). Hence, R_{ddr} is the reflection response at \mathbb{S}_0 , double dereverberated at the source and the receiver side.

Next, we derive the algorithm for retrieving R_{ddr} from the reflection response R . Substitution of equation 63 into equation 73 gives

$$R_{\text{ddr}} = v^{+,+} \Psi_b^v R v^+ \quad (77)$$

Equation 77 accomplishes double dereverberation by double extrapolated focusing. The algorithm is similar to redatuming by double focusing (equation 28), but it is significantly less sensitive to a model of the medium because the sources and receivers stay at the surface.

Substituting equation 61 into equation 77, we obtain

$$R_{\text{ddr}} = \Psi_b^v R - (-\Psi_b^v R \Omega^v) - (-\Omega^{v,t} \Psi_b^v R) - (-\Omega^{v,t} \Psi_b^v R \Omega^v) + \dots \quad (78)$$

with $\Omega^v = \Theta_a^v R^* \Theta_b^v R$. This is a similar expansion as equation 30 for redatuming by double focusing, but it lacks the direct arrival

of the focusing function $f_{1,d}^+$, which requires a macro subsurface model. In theory, equation 78 converges. It allows an adaptive implementation of double dereverberation, to compensate for imperfections in the reflection response. Because the sources and receivers stay at the surface, the output R_{ddr} can be directly compared with the input data R , which is advantageous for quality control. Pereira et al. (2019) apply a modified version of this method to suppress first-order internal multiples from a 3D deep-water ocean-bottom node data set. Reinicke and Dukalski (2020) and Staring et al. (2021) apply the method to shallow water numerical and field data sets, demonstrating the significance of including higher order terms to suppress internal multiples caused by a complex overburden.

Primary retrieval

The dereverberation methods discussed in the previous sections have in common that they remove internal multiples between the acquisition boundary \mathbb{S}_0 and a single predefined boundary \mathbb{S}_A in the subsurface. Here, we discuss a method for eliminating all internal multiples.

Our starting point is equation 63 which, after substitution of equation 61, becomes

$$U_{R,S'}^{-,+} = \Psi_b^v R \sum_{k=0}^K \{\Theta_a^v R^* \Theta_b^v R\}^k \delta \quad (79)$$

This expression shows how to obtain the extrapolated Green's function $U^{-,+}(\mathbf{x}_R, \mathbf{x}'_S, t; x_{3,A})$ from the reflection data $R(\mathbf{x}_R, \mathbf{x}_S, t)$. According to equation 50, this extrapolated Green's function is interpreted as the reflection response between \mathbf{x}'_S and \mathbf{x}_R at the surface \mathbb{S}_0 , in which the wavefield between the source at \mathbf{x}'_S and \mathbb{S}_A (at depth $x_{3,A}$) consists of the direct downgoing wave only; see Figure 8. In equation 53 and Figure 10a, we showed that the first possible arrival of this response, denoted as $\{U^{-,+}(\mathbf{x}_R, \mathbf{x}'_S, t; x_{3,A})\}^{\text{first}}$, is the primary reflection response of a hypothetical reflector directly below \mathbb{S}_A , with the two-way traveltime $t_{\text{d2}}(\mathbf{x}_R, \mathbf{x}'_S; x_{3,A})$. Assuming that the hypothetical reflector has a local reflection coefficient $r(\mathbf{x}_A)$, we may replace equation 53 by

$$\begin{aligned} & \{U^{-,+}(\mathbf{x}_R, \mathbf{x}'_S, t; x_{3,A})\}^{\text{first}} \\ &= \int_{\mathbb{S}_A} d\mathbf{x}_A \int_0^t T_d(\mathbf{x}_R, \mathbf{x}_A, t') r(\mathbf{x}_A) T_d(\mathbf{x}_A, \mathbf{x}'_S, t-t') dt' \end{aligned} \quad (80)$$

When the reflectivity is angle-dependent, $r(\mathbf{x}_A)$ should actually be replaced by a kernel $r(\mathbf{x}'_A, \mathbf{x}_A, t)$, and extra integrals along \mathbb{S}_A and time should be included in equation 80 (Berkhout, 1982; de Bruin et al., 1990). For convenience, we continue with the simple form of equation 80.

We introduce $R_{\text{prm}}(\mathbf{x}_R, \mathbf{x}'_S, t)$ as the primary reflection response of the medium at the surface \mathbb{S}_0 . It can be obtained by evaluating equation 79 for all $x_{3,A}$ and, for each $x_{3,A}$, assigning the time slice $t = t_{\text{d2}}(\mathbf{x}_R, \mathbf{x}'_S; x_{3,A})$ to $R_{\text{prm}}(\mathbf{x}_R, \mathbf{x}'_S, t)$, according to

$$R_{\text{prm}}(\mathbf{x}_R, \mathbf{x}'_S, t_{\text{d2}}) = \{U^{-,+}(\mathbf{x}_R, \mathbf{x}'_S, t; x_{3,A})\}_{t=t_{\text{d2}}(\mathbf{x}_R, \mathbf{x}'_S; x_{3,A})} \quad (81)$$

(van der Neut and Wapenaar, 2016). Because the window Ψ_b^v in equation 79 passes the selected time slice, we may remove this

window function from this equation when its output $U^{-,+}$ is used in equation 81. When $x_{3,A}$ corresponds to the depth of an interface, then, according to equation 80, $R_{\text{prm}}(\mathbf{x}_R, \mathbf{x}'_S, t_{d2})$ for the corresponding two-way traveltimes t_{d2} represents the primary reflection response of that interface. When there is no interface at $x_{3,A}$, then $R_{\text{prm}}(\mathbf{x}_R, \mathbf{x}'_S, t_{d2})$ will be zero at the corresponding two-way traveltimes t_{d2} . Figure 12 visualizes $R_{\text{prm}}(\mathbf{x}_R, \mathbf{x}'_S, t_{d2})$ for all $x_{3,A}$.

Note that this method still requires an estimate of the velocity model to derive $t_{d2}(\mathbf{x}_R, \mathbf{x}'_S; x_{3,A})$ (which appears in the window function Θ_b^v in equation 79 as well as in equation 81). Furthermore, the time slices for varying $x_{3,A}$ will, in general, not cover the space-time domain $(\mathbf{x}_R, \mathbf{x}'_S, t)$ in a regular way. Both issues can be overcome by replacing the depth variable $x_{3,A}$ by the two-way traveltimes t_2 along the vertical coordinate between $x_{3,0}$ and $x_{3,A}$ (hence, independently of \mathbf{x}_R and \mathbf{x}'_S), and by replacing the time window functions $\Theta_{a,b}^v(\mathbf{x}_R, \mathbf{x}'_S, t; x_{3,A})$ by

$$\bar{\Theta}_a^v(t; t_2) = \theta(t - \epsilon), \quad (82)$$

$$\bar{\Theta}_b^v(t; t_2) = \theta(t_2 - \epsilon - t) \quad (83)$$

(Zhang et al., 2019a). Making these replacements in equations 79 and 81, we obtain

$$R_{\text{prm}}(\mathbf{x}_R, \mathbf{x}'_S, t_2) = \{U^{-,+}(\mathbf{x}_R, \mathbf{x}'_S, t; t_2)\}_{t=t_2} = \left(R \sum_{k=0}^K \{ \bar{\Theta}_a^v R^* \bar{\Theta}_b^v R \}^k \delta \right)_{t=t_2}. \quad (84)$$

This equation shows how the primary reflection response $R_{\text{prm}}(\mathbf{x}_R, \mathbf{x}'_S, t_2)$ (called R_t by Zhang et al., 2019a) is retrieved from the reflection data at the surface without needing any velocity information. Note that the space-independent window function $\bar{\Theta}_b^v$ cuts through offset-dependent events in the data. This aspect of the method is analyzed in detail by Thorbecke et al. (2021). For a field data example, we refer readers to Zhang and Slob (2020b).

Transmission-loss compensated primary retrieval

In the ‘‘Receiver-side dereverberation by MDD’’ section, we showed that the response $\tilde{R}_{\text{dr}}^{\text{uc}}$, which is obtained by MDD,

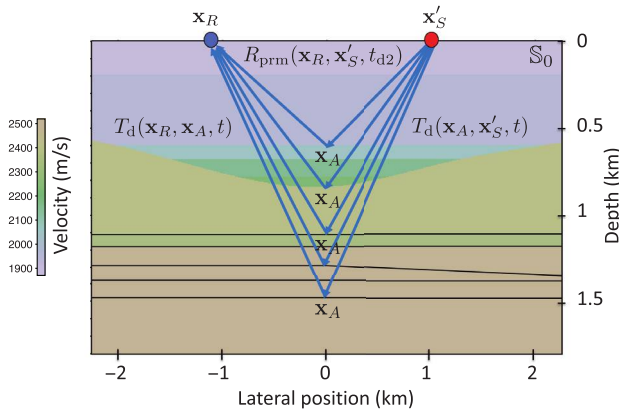


Figure 12. Visualization of the primary response $R_{\text{prm}}(\mathbf{x}_R, \mathbf{x}'_S, t_{d2})$, obtained from equations 79, 80, and 81 for all $x_{3,A}$.

is compensated for the transmission losses between \mathbb{S}_0 and \mathbb{S}_A (Figure 11a). Slob et al. (2014) show for the 1D situation that a transmission-loss compensated local reflection coefficient can be obtained directly from the upgoing focusing function f_1^- , hence, without the need for deconvolution. Using the extrapolation method, it thus follows that a transmission-loss compensated primary reflection response at the surface of a local reflection event in the subsurface can be obtained directly from the extrapolated upgoing focusing function v^- . This idea was used by Zhang et al. (2019b), who developed a 3D method for retrieving the transmission-loss compensated primary response at the surface for all reflectors in the subsurface, without the need for MDD. Here, we discuss this approach in detail.

Before we analyze the extrapolated upgoing focusing function v^- , we discuss focusing functions $f_2^+(\mathbf{x}, \mathbf{x}_R, t)$ and $f_2^-(\mathbf{x}, \mathbf{x}_R, t)$, with \mathbf{x}_R at \mathbb{S}_0 , as counterparts of $f_1^+(\mathbf{x}, \mathbf{x}_A, t)$ and $f_1^-(\mathbf{x}, \mathbf{x}_A, t)$, with \mathbf{x}_A at \mathbb{S}_A . These focusing functions are defined in the same truncated medium; see Figure 13. The upgoing focusing function $f_2^-(\mathbf{x}_B, \mathbf{x}_R, t)$, with \mathbf{x}_B at \mathbb{S}_A , is defined such that $f_2^-(\mathbf{x}, \mathbf{x}_R, t)$ focuses at $\mathbf{x} = \mathbf{x}_R$ and $t = 0$ and continues as a diverging upgoing field into the homogeneous half-space above \mathbb{S}_0 . The formal focusing conditions are

$$f_2^+(\mathbf{x}'_R, \mathbf{x}_R, t) = 0, \quad (85)$$

$$f_2^-(\mathbf{x}'_R, \mathbf{x}_R, t) = \delta(\mathbf{x}'_{H,R} - \mathbf{x}_{H,R})\delta(t), \quad (86)$$

for \mathbf{x}'_R at \mathbb{S}_0 . The downgoing focusing function $f_2^+(\mathbf{x}_A, \mathbf{x}_R, t)$ is the response of the truncated medium to $f_2^-(\mathbf{x}_B, \mathbf{x}_R, t)$, observed at \mathbf{x}_A at \mathbb{S}_A . This is formulated as

$$f_2^+(\mathbf{x}_A, \mathbf{x}_R, t) = \int_{\mathbb{S}_A} d\mathbf{x}_B \int_0^\infty R^\cap(\mathbf{x}_A, \mathbf{x}_B, t') f_2^-(\mathbf{x}_B, \mathbf{x}_R, t - t') dt', \quad (87)$$

where $R^\cap(\mathbf{x}_A, \mathbf{x}_B, t)$ is the reflection response of the truncated medium ‘‘from below.’’ The following relations hold between f_1^\pm and f_2^\pm (Wapenaar et al., 2014):

$$f_1^+(\mathbf{x}_R, \mathbf{x}_A, t) = f_2^-(\mathbf{x}_A, \mathbf{x}_R, t), \quad (88)$$

$$f_1^-(\mathbf{x}_R, \mathbf{x}_A, t) = -f_2^+(\mathbf{x}_A, \mathbf{x}_R, -t). \quad (89)$$

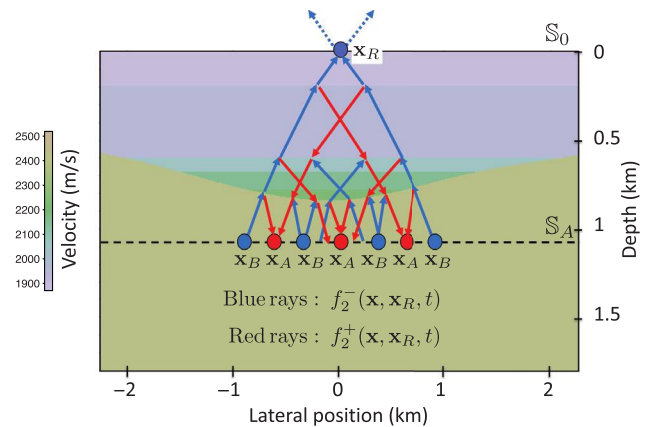


Figure 13. Focusing functions f_2^- and f_2^+ in the truncated medium.

We now analyze the extrapolated upgoing focusing function $v^-(\mathbf{x}_R, \mathbf{x}'_S, t; x_{3,A})$, as defined by equation 49. Upon substitution of equation 89, we obtain

$$v^-(\mathbf{x}_R, \mathbf{x}'_S, t; x_{3,A}) = - \int_{\mathbb{S}_A} d\mathbf{x}_A \int_{-\infty}^t f_2^+(\mathbf{x}_A, \mathbf{x}_R, -t') T_d(\mathbf{x}_A, \mathbf{x}'_S, t-t') dt'. \quad (90)$$

In the compact operator notation, this equation reads

$$v^- = -f_2^{+*} T_d. \quad (91)$$

For f_2^+ , we use equation 87 in which we substitute equation 88. This gives

$$f_2^+ = R^\Omega f_1^{+t}. \quad (92)$$

Substituting this into equation 91, using $R^{\Omega t} = R^\Omega$, yields

$$v^- = -f_1^{+*} R^{\Omega*} T_d. \quad (93)$$

The last event of v^- is obtained by selecting the first events of R^Ω and f_1^+ ; hence,

$$v_{\text{last}}^- = -f_{1,d}^{+*} R_{\text{first}}^{\Omega*} T_d, \quad (94)$$

or, using equation 17,

$$v_{\text{last}}^- = -(T_d^*)^{-1} R_{\text{first}}^{\Omega*} T_d. \quad (95)$$

Here, $(T_d^*)^{-1}$ is the transmission-loss compensated direct wave; see the discussion following equation 70. Equation 95 is visualized in Figure 14a. This figure shows that $\{v^-(\mathbf{x}_R, \mathbf{x}'_S, t; x_{3,A})\}_{\text{last}}$ is interpreted as a reflection response between \mathbf{x}'_S and \mathbf{x}_R at the surface \mathbb{S}_0 , in which the wavefields between \mathbb{S}_0 and \mathbb{S}_A consist of direct downgoing and transmission-loss compensated upgoing waves only, and the only reflection comes from the lower side of the last interface above \mathbb{S}_A . Next, we express R_{first}^Ω as

$$R_{\text{first}}^\Omega(\mathbf{x}_B, \mathbf{x}_A, t) = - \int_{\mathbb{S}_{\text{last}}} d\mathbf{x} \int_0^t w(\mathbf{x}_B, \mathbf{x}, t') r(\mathbf{x}) w(\mathbf{x}, \mathbf{x}_A, t-t') dt', \quad (96)$$

where \mathbb{S}_{last} represents the last interface of the truncated medium, $w(\mathbf{x}, \mathbf{x}_A, t)$ is an extrapolation operator for the homogeneous layer between \mathbb{S}_A and \mathbb{S}_{last} , and $r(\mathbf{x})$ with \mathbf{x} on \mathbb{S}_{last} is the local reflection coefficient of the last interface. The minus sign accounts for the fact that, in the acoustic approximation, the reflection coefficient at the lower side of an interface is the opposite of that at the upper side of the same interface. In the compact operator notation, equation 96 becomes

$$R_{\text{first}}^\Omega = -w^t r_{\text{last}} w. \quad (97)$$

Substituting this into equation 95, using the fact that in the homogeneous layer we have $w^t = (w^*)^{-1}$, we obtain

$$v_{\text{last}}^- = (w T_d^*)^{-1} r_{\text{last}} (w^* T_d). \quad (98)$$

Here, $w^* T_d$ is the direct arrival of the transmission response between \mathbb{S}_0 and \mathbb{S}_A , back-extrapolated from \mathbb{S}_A to \mathbb{S}_{last} , which we denote by $T_{d,\text{last}}$. Hence,

$$v_{\text{last}}^- = (T_{d,\text{last}}^*)^{-1} r_{\text{last}} T_{d,\text{last}}, \quad (99)$$

or

$$\begin{aligned} & \{v^-(\mathbf{x}_R, \mathbf{x}'_S, t; x_{3,A})\}_{\text{last}} \\ &= \int_{\mathbb{S}_{\text{last}}} d\mathbf{x} \int_0^t T_d^{-1}(\mathbf{x}_R, \mathbf{x}, -t') r(\mathbf{x}) T_d(\mathbf{x}, \mathbf{x}'_S, t-t') dt'. \end{aligned} \quad (100)$$

This equation is visualized in Figure 14b. It shows that $\{v^-(\mathbf{x}_R, \mathbf{x}'_S, t; x_{3,A})\}_{\text{last}}$ is the transmission-loss compensated primary reflection response of the last interface above \mathbb{S}_A (see also the discussion following equation 70).

Next, we discuss a Marchenko scheme to retrieve $\{v^-(\mathbf{x}_R, \mathbf{x}'_S, t; x_{3,A})\}_{\text{last}}$ from the reflection response $R(\mathbf{x}_R, \mathbf{x}_S, t)$ at the surface. Equations 51 and 52 form again the basis for this. We need to define window functions that suppress the extrapolated Green's functions U^{-+} and U^{-} from these equations, but preserve v_{last}^- , even when \mathbb{S}_A lies close to the reflector represented by v_{last}^- . If we would choose a hypothetical reflector just below \mathbb{S}_A , like we did in equation 53, this reflector would by definition lie outside the truncated medium and hence not contribute to $v^-(\mathbf{x}_R, \mathbf{x}'_S, t; x_{3,A})$. Instead, we choose a hypothetical reflector just above \mathbb{S}_A (i.e., inside the truncated medium) and define the corresponding event as

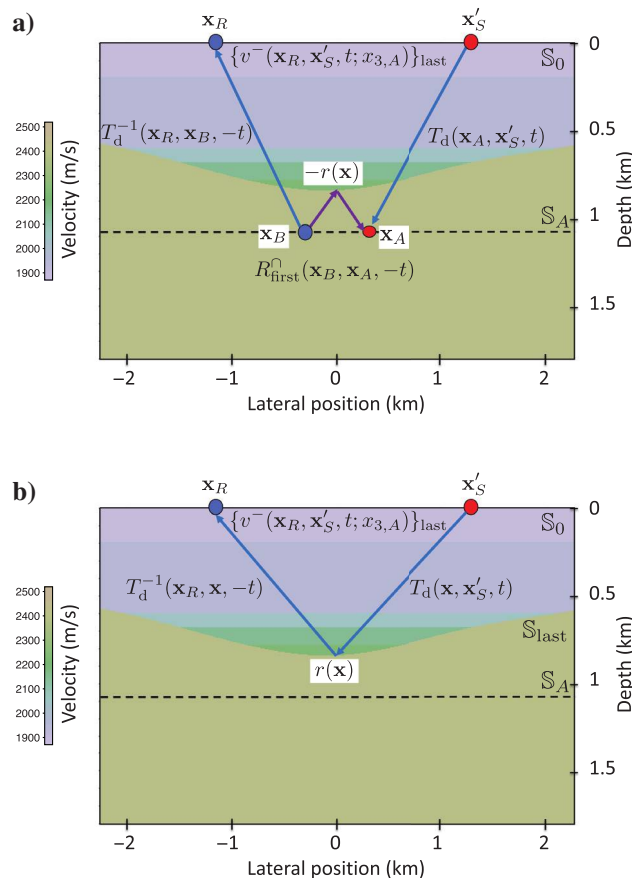


Figure 14. (a) Visualization of equation 95. The purple rays represent the time-reversed reflection response at \mathbb{S}_A of the last reflector of the truncated medium above \mathbb{S}_A . (b) Visualization of equation 100 (the transmission-loss compensated primary response of the last interface above \mathbb{S}_A).

$\{v^-(\mathbf{x}_R, \mathbf{x}'_S, t; x_{3,A})\}_{\text{last}}$, with the subscript “last” standing for “last possible.” Note that in this way we are approaching the hypothetical reflector from below, similar to how we approached the actual last reflector from below in equation 95 and Figure 14a. Analogous to equation 100, we write

$$\begin{aligned} & \{v^-(\mathbf{x}_R, \mathbf{x}'_S, t; x_{3,A})\}_{\text{last}'} \\ &= \int_{\mathbb{S}_A} d\mathbf{x}_A \int_0^t T_d^{-1}(\mathbf{x}_R, \mathbf{x}_A, -t') r(\mathbf{x}_A) T_d(\mathbf{x}_A, \mathbf{x}'_S, t - t') dt', \quad (101) \end{aligned}$$

where $r(\mathbf{x}_A)$ is the reflection coefficient of the hypothetical reflector. The arrival time of this event is again the two-way traveltime $t_{d2}(\mathbf{x}_R, \mathbf{x}'_S; x_{3,A})$. Hence, if we apply a time window to equation 51 that removes everything beyond $t = t_b = t_{d2}(\mathbf{x}_R, \mathbf{x}'_S; x_{3,A}) + \epsilon$, then $v_{\text{last}'}^-$ is preserved (and, due to the finite bandwidth, it is still preserved when \mathbb{S}_A lies less than half a wavelength above the hypothetical reflector [Zhang et al., 2019b]). We define this time window as

$$\Theta_b^{\epsilon,v}(\mathbf{x}_R, \mathbf{x}'_S, t; x_{3,A}) = \theta(t_b - t) = \theta(t_{d2} + \epsilon - t). \quad (102)$$

Because we replaced $t_{d2} - \epsilon$ from our previous window function (equation 56) by $t_{d2} + \epsilon$, the question arises whether this window still suppresses $U^{-,+}(\mathbf{x}_R, \mathbf{x}'_S, t; x_{3,A})$. To address this question, consider Figure 8 and keep in mind that \mathbf{x}_A lies just below the hypothetical reflector. Because the virtual source at \mathbf{x}_A radiates downward, the hypothetical reflector does not contribute to $U^{-,+}(\mathbf{x}_R, \mathbf{x}'_S, t; x_{3,A})$. Hence, the first event in $U^{-,+}$ arrives later than $t_{d2}(\mathbf{x}_R, \mathbf{x}'_S; x_{3,A}) + \epsilon$ (still assuming that the layers are not thin compared to the wavelength), so the proposed time window indeed suppresses $U^{-,+}(\mathbf{x}_R, \mathbf{x}'_S, t; x_{3,A})$ from equation 51. To suppress $U^{-,-}(\mathbf{x}_R, \mathbf{x}'_S, -t; x_{3,A})$ from equation 52, again we need the time window $\Theta_a^v(\mathbf{x}_R, \mathbf{x}'_S, t; x_{3,A})$ defined in equation 55, which removes everything before $t = t_a = t_0(\mathbf{x}_R, \mathbf{x}'_S) + \epsilon$. Applying the windows $\Theta_b^{\epsilon,v}$ and Θ_a^v to equations 51 and 52, we obtain, analogous to equations 59 and 61,

$$v^-(\mathbf{x}_R, \mathbf{x}'_S, t; x_{3,A}) = \Theta_b^{\epsilon,v} R \sum_{k=0}^K \{\Theta_a^v R^* \Theta_b^{\epsilon,v} R\}^k \delta. \quad (103)$$

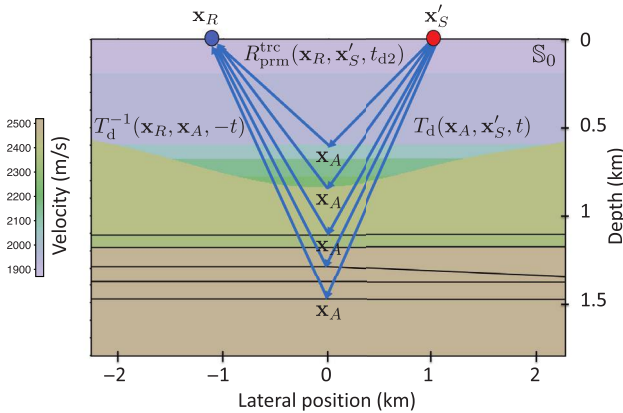


Figure 15. Visualization of the transmission-loss compensated primary response $R_{\text{prm}}^{\text{trc}}(\mathbf{x}_R, \mathbf{x}'_S, t_{d2})$, obtained from equations 101, 103, and 104 for all $x_{3,A}$.

The transmission-loss compensated primary reflection response $R_{\text{prm}}^{\text{trc}}(\mathbf{x}_R, \mathbf{x}'_S, t)$ can be obtained by evaluating equation 103 for all $x_{3,A}$ and, for each $x_{3,A}$, assigning the time slice $t = t_{d2}(\mathbf{x}_R, \mathbf{x}'_S; x_{3,A})$ to $R_{\text{prm}}^{\text{trc}}(\mathbf{x}_R, \mathbf{x}'_S, t)$, according to

$$R_{\text{prm}}^{\text{trc}}(\mathbf{x}_R, \mathbf{x}'_S, t_{d2}) = \{v^-(\mathbf{x}_R, \mathbf{x}'_S, t; x_{3,A})\}_{t=t_{d2}(\mathbf{x}_R, \mathbf{x}'_S; x_{3,A})}. \quad (104)$$

Because the leftmost window $\Theta_b^{\epsilon,v}$ in equation 103 passes the selected time slice, we may remove this window function from this equation when its output v^- is used in equation 104. Figure 15 visualizes $R_{\text{prm}}^{\text{trc}}(\mathbf{x}_R, \mathbf{x}'_S, t_{d2})$ for all $x_{3,A}$.

Next, using similar arguments as in the previous section, we replace the depth variable $x_{3,A}$ by the two-way traveltime t_2 along the vertical coordinate between $x_{3,0}$ and $x_{3,A}$ (independent of \mathbf{x}_R and \mathbf{x}'_S), and the time window functions Θ_a^v and $\Theta_b^{\epsilon,v}$ by $\bar{\Theta}_a^v(t; t_2)$ defined in equation 82 and

$$\bar{\Theta}_b^{\epsilon,v}(t; t_2) = \theta(t_2 + \epsilon - t) \quad (105)$$

(Zhang et al., 2019b). Making these replacements in equations 103 and 104, we obtain

$$\begin{aligned} R_{\text{prm}}^{\text{trc}}(\mathbf{x}_R, \mathbf{x}'_S, t_2) &= \{v^-(\mathbf{x}_R, \mathbf{x}'_S, t; t_2)\}_{t=t_2} \\ &= \left(R \sum_{k=0}^K \{\bar{\Theta}_a^v R^* \bar{\Theta}_b^{\epsilon,v} R\}^k \delta \right)_{t=t_2}. \quad (106) \end{aligned}$$

This equation shows how the transmission-loss compensated primary reflection response $R_{\text{prm}}^{\text{trc}}(\mathbf{x}_R, \mathbf{x}'_S, t_2)$ (called R_r by Zhang et al., 2019b) is retrieved from the reflection data at the surface without needing any velocity information. For numerical examples, we refer readers to Zhang et al. (2019b) and for an efficient implementation to Zhang and Slob (2020a).

Plane-wave primary retrieval

In this section, we integrate the plane-wave approach, introduced in the “Plane-wave redatuming” section, with the transmission-loss compensated primary retrieval approach, introduced in the previous section. In this way, we combine the numerical efficiency gain achieved by the plane-wave approach, with the model-independence of the primary retrieval approach (Meles et al., 2020).

We define the extrapolated plane-wave focusing functions and Green’s functions, analogous to equations 32 and 34, as

$$\tilde{v}^{\pm}(\mathbf{x}_R, \mathbf{p}, t; x_{3,A}) = \int_{\mathbb{S}_0} v^{\pm}(\mathbf{x}_R, \mathbf{x}'_S, t - \mathbf{p} \cdot \mathbf{x}'_{H,S}; x_{3,A}) d\mathbf{x}'_S \quad (107)$$

and

$$\tilde{U}^{\pm}(\mathbf{x}_R, \mathbf{p}, t; x_{3,A}) = \int_{\mathbb{S}_0} U^{\pm}(\mathbf{x}_R, \mathbf{x}'_S, t - \mathbf{p} \cdot \mathbf{x}'_{H,S}; x_{3,A}) d\mathbf{x}'_S. \quad (108)$$

Note that the integration takes place along the extrapolated source positions \mathbf{x}'_S at the surface \mathbb{S}_0 , unlike in equations 32 and 34, where we integrate along the focal points \mathbf{x}_A at \mathbb{S}_A . Hence, the ray parameter vector $\mathbf{p} = (p_1, p_2)$ refers to a plane wave at the surface rather than at the focal depth. For an interpretation of $\tilde{U}^{-,+}(\mathbf{x}_R, \mathbf{p}, t; x_{3,A})$, substitute equation 50 into equation 108. This gives

$$\tilde{U}^{-,+}(\mathbf{x}_R, \mathbf{p}, t; x_{3,A}) = \int_{\mathbb{S}_A} d\mathbf{x}_A \int_0^t G^{-,+}(\mathbf{x}_R, \mathbf{x}_A, t') \tilde{T}_d(\mathbf{x}_A, \mathbf{p}, t-t') dt', \quad (109)$$

with

$$\tilde{T}_d(\mathbf{x}_A, \mathbf{p}, t) = \int_{\mathbb{S}_0} T_d(\mathbf{x}_A, \mathbf{x}'_S, t - \mathbf{p} \cdot \mathbf{x}'_{H,S}) d\mathbf{x}'_S. \quad (110)$$

Hence, $\tilde{U}^{-,+}(\mathbf{x}_R, \mathbf{p}, t; x_{3,A})$ can be interpreted as the reflection response to a downgoing plane wave with ray parameter \mathbf{p} at the surface \mathbb{S}_0 , observed by a receiver at \mathbf{x}_R , in which the downgoing wave between the surface \mathbb{S}_0 and \mathbb{S}_A consists of the direct downgoing wave only. This is visualized in Figure 16a.

Applying equations 107 and 108 to the left and right sides of equations 51 and 52, we obtain

$$\begin{aligned} & \tilde{U}^{-,+}(\mathbf{x}_R, \mathbf{p}, t; x_{3,A}) + \tilde{v}^{-}(\mathbf{x}_R, \mathbf{p}, t; x_{3,A}) \\ &= \int_{\mathbb{S}_0} d\mathbf{x}_S \int_0^\infty R(\mathbf{x}_R, \mathbf{x}_S, t') \\ & \quad \times \tilde{v}^{+}(\mathbf{x}_S, \mathbf{p}, t-t'; x_{3,A}) dt' \end{aligned} \quad (111)$$

and

$$\begin{aligned} & \tilde{U}^{-,-}(\mathbf{x}_R, -\mathbf{p}, -t; x_{3,A}) + \tilde{v}^{+}(\mathbf{x}_R, \mathbf{p}, t; x_{3,A}) \\ &= \int_{\mathbb{S}_0} d\mathbf{x}_S \int_{-\infty}^0 R(\mathbf{x}_R, \mathbf{x}_S, -t') \\ & \quad \times \tilde{v}^{-}(\mathbf{x}_S, \mathbf{p}, t-t'; x_{3,A}) dt'. \end{aligned} \quad (112)$$

The functions on the left sides of equations 111 and 112, convolved with a wavelet, are shown in gray-level display in Figure 16b and 16c, respectively.

We need time windows that separate the extrapolated plane-wave Green's functions from the extrapolated plane-wave focusing functions in equations 111 and 112. Similar to the primary retrieval methods for extrapolated point sources, we can follow two approaches. If we would design a window $\tilde{\Theta}_b^v$ that suppresses $\tilde{U}^{-,+}(\mathbf{x}_R, \mathbf{p}, t; x_{3,A})$ from equation 111, including its first possible arrival from a hypothetical reflector just below \mathbb{S}_A , then, following an approach similar to that in the ‘‘Primary retrieval’’ section, we would obtain a method for plane-wave primary retrieval, without compensation for transmission losses. However, if we design a window $\tilde{\Theta}_b^{e,v}$ that preserves $\tilde{v}^{-}(\mathbf{x}_R, \mathbf{p}, t; x_{3,A})$ in equation 111, including its last possible arrival from a hypothetical reflector just above \mathbb{S}_A , then an approach similar to that in the ‘‘Transmission-loss compensated primary retrieval’’ section will lead to a method for plane-wave transmission-loss compensated primary retrieval. Here we only discuss the second approach in more detail. Substituting equation 101 into equation 107, we obtain

$$\begin{aligned} & \{\tilde{v}^{-}(\mathbf{x}_R, \mathbf{p}, t; x_{3,A})\}_{\text{last}^-} \\ &= \int_{\mathbb{S}_A} d\mathbf{x}_A \int_0^t T_d^{-1}(\mathbf{x}_R, \mathbf{x}_A, -t') r(\mathbf{x}_A) \tilde{T}_d(\mathbf{x}_A, \mathbf{p}, t-t') dt'. \end{aligned} \quad (113)$$

This is interpreted as the transmission-loss compensated primary reflection response to a dipping plane wave emitted from \mathbb{S}_0 with ray parameter \mathbf{p} and arriving at \mathbf{x}_R via a hypothetical reflector just above \mathbb{S}_A . We denote the arrival time of this event as $\tilde{t}_{d2}(\mathbf{x}_R, \mathbf{p}; x_{3,A})$. Hence, if we apply a time window to equation 111 that removes everything beyond $t = t_b = \tilde{t}_{d2}(\mathbf{x}_R, \mathbf{p}; x_{3,A}) + \epsilon$ (the dashed line in Figure 16b), then $\{\tilde{v}^{-}(\mathbf{x}_R, \mathbf{p}, t; x_{3,A})\}_{\text{last}^-}$ is preserved (note that in this specific example the actual last reflector above \mathbb{S}_A is not close to \mathbb{S}_A in Figure 16a; hence, the last event of $\tilde{v}^{-}(\mathbf{x}_R, \mathbf{p}, t; x_{3,A})$ in Figure 16b is not close to the dashed line).

The window for equation 112 will be designed such that it suppresses $\tilde{U}^{-,-}(\mathbf{x}_R, -\mathbf{p}, -t; x_{3,A})$. Substituting equation 54 into equation 108 gives

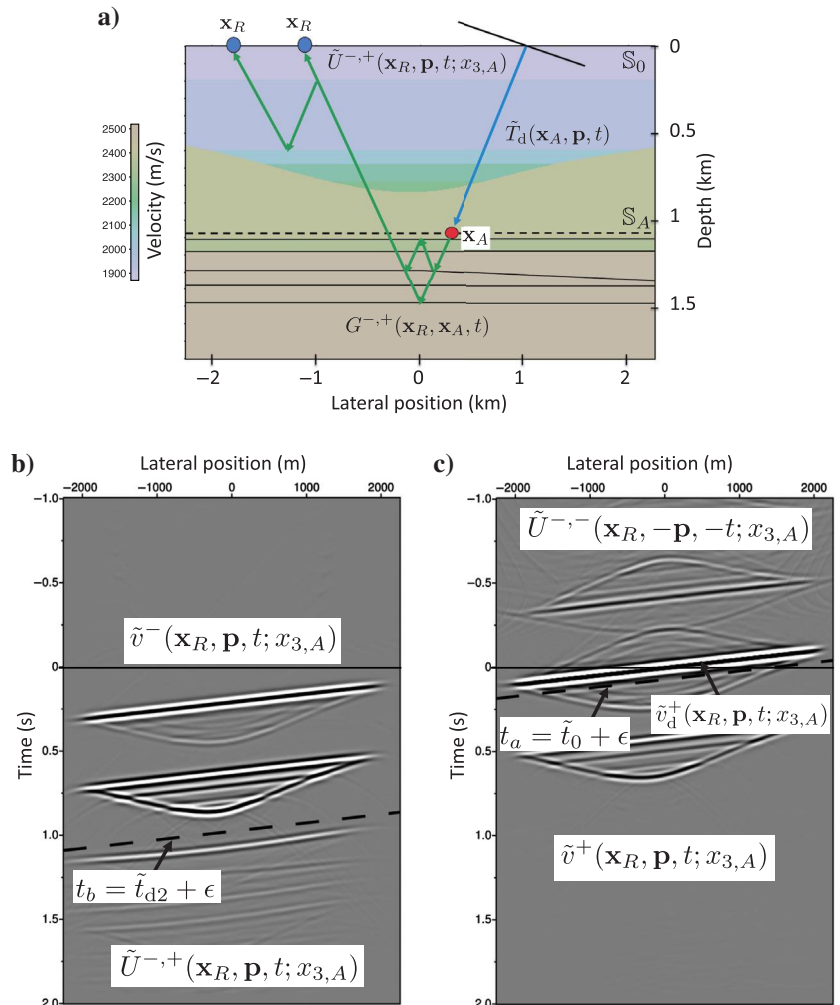


Figure 16. (a) Visualization of the extrapolated plane-wave Green's function $\tilde{U}^{-,+}(\mathbf{x}_R, \mathbf{p}, t; x_{3,A})$ (here shown for a negative value of p_1 and $p_2 = 0$). (b) The left side of equation 111 (fixed \mathbf{p} , variable \mathbf{x}_R). (c) The left side of equation 112.

$$\begin{aligned} & \{\tilde{U}^{-}(\mathbf{x}_R, -\mathbf{p}, -t; x_{3,A})\}_{\text{last}} \\ &= - \int_{\mathbb{S}_A} d\mathbf{x}_A \int_{-\infty}^0 T_d(\mathbf{x}_R, \mathbf{x}_A, -t') \tilde{T}_d(\mathbf{x}_A, \mathbf{p}, t - t') dt'. \end{aligned} \quad (114)$$

This is interpreted as the back-extrapolation of the plane-wave response $\tilde{T}_d(\mathbf{x}_A, \mathbf{p}, t)$ from \mathbb{S}_A to \mathbb{S}_0 , which gives the original plane wave at \mathbb{S}_0 with ray parameter \mathbf{p} . The arrival time of this event is $\tilde{t}_0(\mathbf{x}_R, \mathbf{p}) = \mathbf{p} \cdot \mathbf{x}_{H,R}$. Hence, $\tilde{U}^{-}(\mathbf{x}_R, -\mathbf{p}, -t; x_{3,A})$ can be suppressed from equation 112 by a time window that removes everything before $t = t_a = \mathbf{p} \cdot \mathbf{x}_{H,R} + \epsilon$ (the dashed line in Figure 16c, indicated by $\tilde{t}_0 + \epsilon$). We define the two time windows as

$$\tilde{\Theta}_a^v(\mathbf{x}_R, \mathbf{p}, t; x_{3,A}) = \theta(t - \mathbf{p} \cdot \mathbf{x}_{H,R} - \epsilon), \quad (115)$$

$$\tilde{\Theta}_b^{\epsilon,v}(\mathbf{x}_R, \mathbf{p}, t; x_{3,A}) = \theta(\tilde{t}_{d2} + \epsilon - t). \quad (116)$$

These windows pass the extrapolated plane-wave focusing functions \tilde{v}^+ and \tilde{v}^- , except the extrapolated plane-wave direct arrival $\tilde{v}_d^+(\mathbf{x}_R, \mathbf{p}, t; x_{3,A})$, which coincides with the last arrival of $\tilde{U}^{-}(\mathbf{x}_R, -\mathbf{p}, -t; x_{3,A})$; see Figure 16c. By substituting equation 58 into equation 107, we obtain

$$\tilde{v}_d^+(\mathbf{x}_R, \mathbf{p}, t; x_{3,A}) = \delta(t - \mathbf{p} \cdot \mathbf{x}_{H,R}). \quad (117)$$

Application of the time windows to both sides of equations 111 and 112 gives, in the compact operator notation,

$$\tilde{v}^- = \tilde{\Theta}_b^{\epsilon,v} R \tilde{v}^+, \quad (118)$$

$$\tilde{v}^+ = \tilde{\Theta}_a^v R^* \tilde{v}^- + \tilde{\delta}, \quad (119)$$

where $\tilde{\delta}$ stands for $\tilde{v}_d^+(\mathbf{x}_R, \mathbf{p}, t; x_{3,A}) = \delta(t - \mathbf{p} \cdot \mathbf{x}_{H,R})$. Solving these Marchenko equations for the extrapolated plane-wave focusing function \tilde{v}^- yields

$$\tilde{v}^-(\mathbf{x}_R, \mathbf{p}, t; x_{3,A}) = \tilde{\Theta}_b^{\epsilon,v} R \sum_{k=0}^K \{ \tilde{\Theta}_a^v R^* \tilde{\Theta}_b^{\epsilon,v} R \}^k \tilde{\delta}. \quad (120)$$

The plane-wave transmission-loss compensated primary reflection response $\tilde{R}_{\text{prm}}^{\text{trc}}(\mathbf{x}_R, \mathbf{p}, t)$ can be obtained by evaluating equation 120 for all $x_{3,A}$ and, for each $x_{3,A}$, assigning the time slice $t = \tilde{t}_{d2}(\mathbf{x}_R, \mathbf{p}; x_{3,A})$ to $\tilde{R}_{\text{prm}}^{\text{trc}}(\mathbf{x}_R, \mathbf{p}, t)$, according to

$$\tilde{R}_{\text{prm}}^{\text{trc}}(\mathbf{x}_R, \mathbf{p}, \tilde{t}_{d2}) = \{ \tilde{v}^-(\mathbf{x}_R, \mathbf{p}, t; x_{3,A}) \}_{t=\tilde{t}_{d2}(\mathbf{x}_R, \mathbf{p}; x_{3,A})}. \quad (121)$$

Because the leftmost window $\tilde{\Theta}_b^{\epsilon,v}$ in equation 120 passes the selected time slice, we may remove this window function from this equation when its output \tilde{v}^- is used in equation 121. Figure 17 visualizes $\tilde{R}_{\text{prm}}^{\text{trc}}(\mathbf{x}_R, \mathbf{p}, \tilde{t}_{d2})$ for all $x_{3,A}$.

Next, using similar arguments as in the previous section, we replace the depth variable $x_{3,A}$ again by the two-way travelttime t_2 along the vertical coordinate between $x_{3,0}$ and $x_{3,A}$ (hence, independent of \mathbf{x}_R and \mathbf{p}), and the time window function $\tilde{\Theta}_b^{\epsilon,v}(\mathbf{x}_R, \mathbf{p}, t; x_{3,A})$ by

$$\tilde{\Theta}_b^{\epsilon,v}(\mathbf{x}_R, \mathbf{p}, t; t_2) = \theta(t_2 + \mathbf{p} \cdot \mathbf{x}_{H,R} + \epsilon - t) \quad (122)$$

(Meles et al., 2020). Making these replacements in equations 120 and 121, we obtain

$$\begin{aligned} \tilde{R}_{\text{prm}}^{\text{trc}}(\mathbf{x}_R, \mathbf{p}, \tilde{t}_2) &= \{ \tilde{v}^-(\mathbf{x}_R, \mathbf{p}, t; t_2) \}_{t=t_2 + \mathbf{p} \cdot \mathbf{x}_{H,R}} \\ &= \left(R \sum_{k=0}^K \{ \tilde{\Theta}_a^v R^* \tilde{\Theta}_b^{\epsilon,v} R \}^k \tilde{\delta} \right)_{t=t_2 + \mathbf{p} \cdot \mathbf{x}_{H,R}}. \end{aligned} \quad (123)$$

This equation shows how the plane-wave transmission-loss compensated primary reflection response $\tilde{R}_{\text{prm}}^{\text{trc}}(\mathbf{x}_R, \mathbf{p}, \tilde{t}_2)$, with $\tilde{t}_2 = t_2 + \mathbf{p} \cdot \mathbf{x}_{H,R}$, is retrieved from the reflection data at the surface without needing any velocity information. Using this equation as the basis for primary retrieval, the Marchenko method is only needed to retrieve the extrapolated plane-wave focusing function \tilde{v}^- for a limited number of ray parameters at each vertical travelttime. This implies a significant efficiency gain in comparison with primary retrieval based on equation 106, particularly for 3D applications. Meles et al. (2020) discuss applications of plane-wave transmission-loss compensated primary retrieval to 2D numerically modeled data.

DISCUSSION

The past decade has seen vigorous progress in the field of Marchenko equation-based methods for dealing with internal multiples, be it through redatuming and imaging or multiple elimination at the surface. The geophysical community has managed to move from understanding the fundamentals and expanding on them, through identifying (and resolving) some limitations, to making this suite of methods more user-friendly and more computationally efficient and, finally, to apply them to field data. It is therefore prudent to not only take stock of the collective accomplishments of our community, but also to draw a roadmap of attention-worthy research directions. Of those that we were able to identify, we decided to split them up into four main themes: (1) understanding the effects of band limitation, (2) investigating whether the focusing functions or dereverberation operators can be reliably extracted from reflection data for complex subsurface configurations, (3) understanding

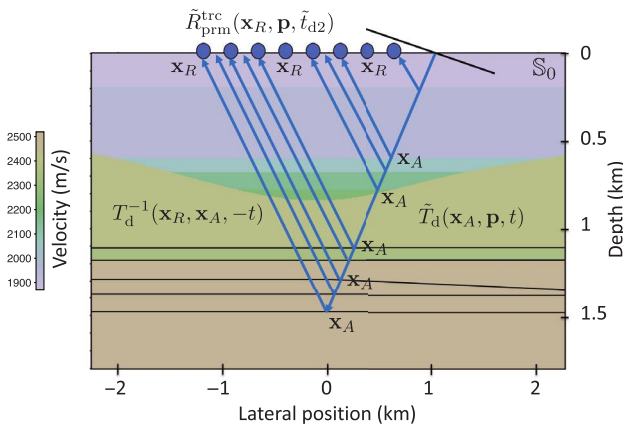


Figure 17. Visualization of the plane-wave transmission-loss compensated primary response $\tilde{R}_{\text{prm}}^{\text{trc}}(\mathbf{x}_R, \mathbf{p}, \tilde{t}_{d2})$, obtained from equations 113, 120, and 121 for all $x_{3,A}$.

how the methods fit within a wider data processing workflow and what quality control tools would be needed, and, finally (4) looking beyond the acoustic assumption outlined in this work.

- 1) We need to close the gap between the theory and real-world applications, in which the signal bandwidth often tends to be much lower than that of the heterogeneities. This is particularly an issue because finite bandwidth and temporal truncations do not go well together. For example, [Elison et al. \(2020\)](#) show with a numerical example that when the scattering is sufficiently high and band-limited data are used, the focusing functions or dereverberation operators are not recovered with full fidelity. Recently, augmentation to the Marchenko theory suggested the use of additional constraints to further improve the quality of the retrieved solutions. However, the current implementation of this extension has, to date, only been shown to work in horizontally layered media. As discussed in [Dukalski \(2020\)](#), the critical minimum-phase reconstruction step can become challenging beyond 1.5D applications, hence requiring further algorithmic developments.
- 2) For complex subsurface configurations, events originating from deep sections may outpace the ones from upshallow. This makes retrieving focusing functions or dereverberation operators directly from the reflection data rather difficult. It would be worthwhile to investigate such situations when one can show that the operators do or do not exist, and to what extent they can be extracted from the reflection data using the data-driven approaches discussed in this work. It might further be worth understanding, should a partially correct operator be found using the schemes we outline here, to what extent it is capable of actually removing the multiples in these complex situations.
- 3) A large-scale deployment of this methodology will be naturally contingent on one's ability to integrate any of the outlined schemes in the data processing workflow (be it for seismic or medical imaging, or otherwise). For instance, when applied in the subsurface imaging workflow, any application should be preceded by surface-related multiple attenuation (with the exception of deepwater settings), or at least a correct wavelet deconvolution step. Because the Marchenko methods rely on sufficient amplitude fidelity of the input data, the strengths and weaknesses of the preprocessing need to be well understood and taken into account. Considering the richness in the physics and scattering relations underpinning the Marchenko method, perhaps physics can also be used as a viable quality control step. This will be particularly important in cases in which multiples are expressed by a massive collection of interfering events, produced by countless reflectors in the subsurface, and in which the interpretation of the generation mechanism of multiples and their order might be very difficult. Perhaps machine learning and/or artificial intelligence applications could be of help. Controlled studies on increasingly complex and realistic numerical data would be very useful in achieving this larger goal.
- 4) Finally, next to a surge of publications covering many aspects of the acoustic theory, developments also include viscoacoustic ([Slob, 2016](#)) and elastic theory ([da Costa Filho et al., 2014](#); [Wapenaar and Slob, 2014](#); [Reinicke et al., 2020](#)). In either of these cases, however, we do not directly measure all data necessary for the algorithms, but perhaps additional constraints

could help move these developments forward. Moreover, in the viscoacoustic and elastic settings, the aforementioned band-limitation issues become even more apparent because so-called “fast converted multiples,” dissipation, and short-period scattering manifest themselves in a similar manner, but have completely different origins and hence might need to be handled by different means. Alternatively, if it is not possible to address one or more of these issues, it will be worth exploring in what parameter regime the acoustic approach performs acceptably ([Reinicke et al., 2021](#)) and, when it fails, how one would know, in practice, that it does (e.g., due to the appearance of some characteristic noise). Further extensions of the theory to increasingly “exotic” systems might also come with the added benefit of bringing to light certain elements that would otherwise be easily missed in simpler methods.

Most of the issues mentioned here apply also to other internal multiple elimination methods. We hope that this paper will contribute to an unprejudiced discussion between the proponents of the different methods that will help to move the interesting field of internal multiple elimination forward.

CONCLUSION

We have presented recent developments of the Marchenko method for geophysical applications in a systematic way. We distinguished two classes of Marchenko methods. The first class of methods, which we call Marchenko redatuming and imaging, aims at creating virtual sources and receivers in the subsurface, from reflection data at the surface. The responses between these virtual sources and receivers are free of internal multiples related to the overburden and can subsequently be used for multiple-free imaging. Methods in the second class also eliminate internal multiples, but the sources and receivers stay at the surface. We refer to these methods as Marchenko multiple elimination. Whereas Marchenko redatuming and imaging methods require a macro model of the subsurface (to define the direct arrival of the Green's functions), Marchenko multiple elimination methods do not need this kind of information. We have used a systematic presentation and unified notation to reveal the relation between the different Marchenko methods in both classes. Finally, we discussed open problems of Marchenko methods (and other internal multiple elimination methods) and indicated new research directions.

ACKNOWLEDGMENTS

We thank the associate editor and reviewers for their positive and constructive reviews, which helped to improve the paper. We acknowledge funding from the European Research Council (ERC) under the European Union's Horizon 2020 research and innovation programme (grant agreement no.: 742703).

DATA AND MATERIALS AVAILABILITY

No data have been used for this study.

REFERENCES

- Amundsen, L., 2001, Elimination of free-surface related multiples without need of the source wavelet: *Geophysics*, **66**, 327–341, doi: [10.1190/1.1444912](https://doi.org/10.1190/1.1444912).

- Bakulin, A., and R. Calvert, 2006, The virtual source method: Theory and case study: *Geophysics*, **71**, no. 4, S1139–S1150, doi: [10.1190/1.2216190](https://doi.org/10.1190/1.2216190).
- Becker, T. S., M. Ravasi, D. J. van Manen, F. Brogini, and J. O. A. Robertsson, 2018, Sparse inversion of the coupled Marchenko equations for simultaneous source wavelet and focusing functions estimation: 80th Annual International Conference and Exhibition, EAGE, Extended Abstracts, Th–P9–15, doi: [10.3997/2214-4609.201801661](https://doi.org/10.3997/2214-4609.201801661).
- Behura, J., K. Wapenaar, and R. Snieder, 2014, Autofocus imaging: Image reconstruction based on inverse scattering theory: *Geophysics*, **79**, no. 3, A19–A26, doi: [10.1190/geo2013-0398.1](https://doi.org/10.1190/geo2013-0398.1).
- Berkhout, A. J., 1982, Seismic migration. Imaging of acoustic energy by wave field extrapolation. A. Theoretical aspects: Elsevier.
- Berkhout, A. J., and D. W. van Wulfften Palthe, 1979, Migration in terms of spatial deconvolution: *Geophysical Prospecting*, **27**, 261–291, doi: [10.1111/j.1365-2478.1979.tb00970.x](https://doi.org/10.1111/j.1365-2478.1979.tb00970.x).
- Berkhout, A. J., and D. J. Verschuur, 1997, Estimation of multiple scattering by iterative inversion — Part 1: Theoretical considerations: *Geophysics*, **62**, 1586–1595, doi: [10.1190/1.1444261](https://doi.org/10.1190/1.1444261).
- Berkhout, A. J., and C. P. A. Wapenaar, 1993, A unified approach to acoustical reflection imaging — Part 2: The inverse problem: *Journal of the Acoustical Society of America*, **93**, 2017–2023, doi: [10.1121/1.406715](https://doi.org/10.1121/1.406715).
- Berryhill, J. R., 1984, Wave-equation datuming before stack: *Geophysics*, **49**, 2064–2066, doi: [10.1190/1.1441620](https://doi.org/10.1190/1.1441620).
- Brackenhoff, J., J. Thorbecke, and K. Wapenaar, 2019a, Monitoring of induced distributed double-couple sources using Marchenko-based virtual receivers: *Solid Earth*, **10**, 1301–1319, doi: [10.5194/se-10-1301-2019](https://doi.org/10.5194/se-10-1301-2019).
- Brackenhoff, J., J. Thorbecke, and K. Wapenaar, 2019b, Virtual sources and receivers in the real Earth: Considerations for practical applications: *Journal of Geophysical Research*, **124**, 11802–11821, doi: [10.1029/2019JB018485](https://doi.org/10.1029/2019JB018485).
- Brogini, F., and R. Snieder, 2012, Connection of scattering principles: A visual and mathematical tour: *European Journal of Physics*, **33**, 593–613, doi: [10.1088/0143-0807/33/3/593](https://doi.org/10.1088/0143-0807/33/3/593).
- Brogini, F., R. Snieder, and K. Wapenaar, 2014, Data-driven wavefield focusing and imaging with multidimensional deconvolution: Numerical examples for reflection data with internal multiples: *Geophysics*, **79**, no. 3, WA107–WA115, doi: [10.1190/geo2013-0307.1](https://doi.org/10.1190/geo2013-0307.1).
- Campillo, M., and A. Paul, 2003, Long-range correlations in the diffuse seismic coda: *Science*, **299**, 547–549, doi: [10.1126/science.1078551](https://doi.org/10.1126/science.1078551).
- Chapman, C. H., 1994, Reflection/transmission coefficients reciprocities in anisotropic media: *Geophysical Journal International*, **116**, 498–501, doi: [10.1111/j.1365-246X.1994.tb01811.x](https://doi.org/10.1111/j.1365-246X.1994.tb01811.x).
- Cui, T., J. Rickett, I. Vasconcelos, and B. Veitch, 2020, Target-oriented full-waveform inversion using Marchenko redatumed wavefields: *Geophysical Journal International*, **223**, 792–810, doi: [10.1093/gji/ggaa333](https://doi.org/10.1093/gji/ggaa333).
- da Costa Filho, C. A., M. Ravasi, A. Curtis, and G. A. Meles, 2014, Elastodynamic Green's function retrieval through single-sided Marchenko inverse scattering: *Physical Review E*, **90**, 063201, doi: [10.1103/PhysRevE.90.063201](https://doi.org/10.1103/PhysRevE.90.063201).
- de Bruin, C. G. M., C. P. A. Wapenaar, and A. J. Berkhout, 1990, Angle-dependent reflectivity by means of prestack migration: *Geophysics*, **55**, 1223–1234, doi: [10.1190/1.1442938](https://doi.org/10.1190/1.1442938).
- Dukalski, M., 2020, The role of minimum phase in internal multiple removal: 82nd Annual International Conference and Exhibition, EAGE, Extended Abstracts, WS15–06, doi: [10.3997/2214-4609.202012091](https://doi.org/10.3997/2214-4609.202012091).
- Dukalski, M., and K. de Vos, 2018, Marchenko inversion in a strong scattering regime including surface-related multiples: *Geophysical Journal International*, **212**, 760–776, doi: [10.1093/gji/ggx434](https://doi.org/10.1093/gji/ggx434).
- Dukalski, M., and K. de Vos, 2020, A closed formula for true-amplitude overburden-generated interbed de-multiple: 82nd Annual International Conference and Exhibition, EAGE, Extended Abstracts, Fr–P05–18, doi: [10.3997/2214-4609.202010903](https://doi.org/10.3997/2214-4609.202010903).
- Dukalski, M., E. Mariani, and K. de Vos, 2019, Handling short-period scattering using augmented Marchenko autofocusing: *Geophysical Journal International*, **216**, 2129–2133, doi: [10.1093/gji/ggy544](https://doi.org/10.1093/gji/ggy544).
- Elison, P., M. S. Dukalski, K. de Vos, D. J. van Manen, and J. O. A. Robertsson, 2020, Data-driven control over short-period internal multiples in media with a horizontally layered overburden: *Geophysical Journal International*, **221**, 769–787, doi: [10.1093/gji/ggaa020](https://doi.org/10.1093/gji/ggaa020).
- Frasier, C. W., 1970, Discrete time solution of plane P-SV waves in a plane layered medium: *Geophysics*, **35**, 197–219, doi: [10.1190/1.1440085](https://doi.org/10.1190/1.1440085).
- Gouédard, P., L. Stehly, F. Brenguier, M. Campillo, Y. Colin de Verdière, E. Larose, L. Margerin, P. Roux, F. J. Sánchez-Sesma, N. M. Shapiro, and R. L. Weaver, 2008, Cross-correlation of random fields: Mathematical approach and applications: *Geophysical Prospecting*, **56**, 375–393, doi: [10.1111/j.1365-2478.2007.00684.x](https://doi.org/10.1111/j.1365-2478.2007.00684.x).
- Haindl, C. M., F. Brogini, M. Ravasi, and D.-J. van Manen, 2018, Using sparsity to improve the accuracy of Marchenko imaging given imperfect acquisition geometries: 80th Annual International Conference and Exhibition, EAGE, Extended Abstracts, Th–P9–14, doi: [10.3997/2214-4609.201801660](https://doi.org/10.3997/2214-4609.201801660).
- Ikelle, L. T., 2006, A construct of internal multiples from surface data only: The concept of virtual seismic events: *Geophysical Journal International*, **164**, 383–393, doi: [10.1111/j.1365-246X.2006.02857.x](https://doi.org/10.1111/j.1365-246X.2006.02857.x).
- Jakubowicz, H., 1998, Wave equation prediction and removal of interbed multiples: 68th Annual International Meeting, SEG, Expanded Abstracts, 1527–1530, doi: [10.1190/1.1820204](https://doi.org/10.1190/1.1820204).
- Kennett, B. L. N., N. J. Kerry, and J. H. Woodhouse, 1978, Symmetries in the reflection and transmission of elastic waves: *Geophysical Journal of the Royal Astronomical Society*, **52**, 215–229, doi: [10.1111/j.1365-246X.1978.tb04230.x](https://doi.org/10.1111/j.1365-246X.1978.tb04230.x).
- Lamb, G. L., 1980, Elements of soliton theory: John Wiley and Sons, Inc.
- Luiken, N., and T. van Leeuwen, 2020, Seismic wavefield redatuming with regularized multi-dimensional deconvolution: *Inverse Problems*, **36**, 095010, doi: [10.1088/1361-6420/aba9d1](https://doi.org/10.1088/1361-6420/aba9d1).
- Meles, G. A., K. Wapenaar, and A. Curtis, 2016, Reconstructing the primary reflections in seismic data by Marchenko redatuming and convolutional interferometry: *Geophysics*, **81**, no. 2, Q15–Q26, doi: [10.1190/geo2015-0377.1](https://doi.org/10.1190/geo2015-0377.1).
- Meles, G. A., K. Wapenaar, and J. Thorbecke, 2018, Virtual plane-wave imaging via Marchenko redatuming: *Geophysical Journal International*, **214**, 508–519, doi: [10.1093/gji/ggy143](https://doi.org/10.1093/gji/ggy143).
- Meles, G. A., L. Zhang, J. Thorbecke, K. Wapenaar, and E. Slob, 2020, Data-driven retrieval of primary plane-wave responses: *Geophysical Prospecting*, **68**, 1834–1846, doi: [10.1111/1365-2478.12960](https://doi.org/10.1111/1365-2478.12960).
- Mildner, C., M. Dukalski, P. Elison, K. de Vos, F. Brogini, and J. O. A. Robertsson, 2019, True amplitude-versus-offset Green's function retrieval using augmented Marchenko focusing: 81st Annual International Conference and Exhibition, EAGE, Extended Abstracts, Tu–R04–08, doi: [10.3997/2214-4609.201900839](https://doi.org/10.3997/2214-4609.201900839).
- Mulder, W. A., 2005, Rigorous redatuming: *Geophysical Journal International*, **161**, 401–415, doi: [10.1111/j.1365-246X.2005.02615.x](https://doi.org/10.1111/j.1365-246X.2005.02615.x).
- Peng, H., I. Vasconcelos, Y. Sripanich, and L. Zhang, 2019, On the effects of acquisition sampling on Marchenko-based focusing and primary estimation: 81st Annual International Conference and Exhibition, EAGE, Extended Abstracts, Th–R08–09, doi: [10.3997/2214-4609.201901570](https://doi.org/10.3997/2214-4609.201901570).
- Pereira, R., M. Ramzy, P. Griscenco, B. Huard, H. Huang, L. Cypriano, and A. Khalil, 2019, Internal multiple attenuation for OBN data with overburden/target separation: 89th Annual International Meeting, SEG, Expanded Abstracts, 4520–4524, doi: [10.1190/segam2019-3215138.1](https://doi.org/10.1190/segam2019-3215138.1).
- Ravasi, M., I. Vasconcelos, A. Kritski, A. Curtis, C. A. da Costa Filho, and G. A. Meles, 2016, Target-oriented Marchenko imaging of a North Sea field: *Geophysical Journal International*, **205**, 99–104, doi: [10.1093/gji/ggv528](https://doi.org/10.1093/gji/ggv528).
- Reinicke, C., and M. Dukalski, 2020, Effective media theory consistent multiple elimination with the Marchenko equation based methods: 82nd Annual International Conference and Exhibition, EAGE, Extended Abstracts, Fr–Dome5–01, doi: [10.3997/2214-4609.202010907](https://doi.org/10.3997/2214-4609.202010907).
- Reinicke, C., M. Dukalski, and K. Wapenaar, 2020, Comparison of monotonicity challenges encountered by the inverse scattering series and the Marchenko demultiple method for elastic waves: *Geophysics*, **85**, no. 5, Q11–Q26, doi: [10.1190/geo2019-0674.1](https://doi.org/10.1190/geo2019-0674.1).
- Reinicke, C., M. Dukalski, and K. Wapenaar, 2021, Internal multiple elimination: Can we trust an acoustic approximation? *Geophysics*, **86**, this issue, doi: [10.1190/geo2020-0850.1](https://doi.org/10.1190/geo2020-0850.1).
- Rietveld, W. E. A., A. J. Berkhout, and C. P. A. Wapenaar, 1992, Optimum seismic illumination of hydrocarbon reservoirs: *Geophysics*, **57**, 1334–1345, doi: [10.1190/1.1443200](https://doi.org/10.1190/1.1443200).
- Rose, J. H., 2001, “Single-sided” focusing of the time-dependent Schrödinger equation: *Physical Review A*, **65**, 012707, doi: [10.1103/PhysRevA.65.012707](https://doi.org/10.1103/PhysRevA.65.012707).
- Rose, J. H., 2002, “Single-sided” autofocusing of sound in layered materials: *Inverse Problems*, **18**, 1923–1934, doi: [10.1088/0266-5611/18/6/329](https://doi.org/10.1088/0266-5611/18/6/329).
- Schultz, P. S., and J. F. Claerbout, 1978, Velocity estimation and downward continuation by wavefront synthesis: *Geophysics*, **43**, 691–714, doi: [10.1190/1.1440847](https://doi.org/10.1190/1.1440847).
- Schuster, G. T., J. Yu, J. Sheng, and J. Rickett, 2004, Interferometric/daylight seismic imaging: *Geophysical Journal International*, **157**, 838–852, doi: [10.1111/j.1365-246X.2004.02251.x](https://doi.org/10.1111/j.1365-246X.2004.02251.x).
- Shoja, S. M. A., G. A. Meles, and K. Wapenaar, 2020, A proposal for Marchenko-based target-oriented full waveform inversion: 82nd Annual International Conference and Exhibition, EAGE, Extended Abstracts, 1–5, doi: [10.3997/2214-4609.202011020](https://doi.org/10.3997/2214-4609.202011020).
- Singh, S., R. Snieder, J. van der Neut, J. Thorbecke, E. Slob, and K. Wapenaar, 2017, Accounting for free-surface multiples in Marchenko imaging: *Geophysics*, **82**, no. 1, R19–R30, doi: [10.1190/geo2015-0646.1](https://doi.org/10.1190/geo2015-0646.1).
- Slob, E., 2016, Green's function retrieval and Marchenko imaging in a dispersive acoustic medium: *Physical Review Letters*, **116**, 164301, doi: [10.1103/PhysRevLett.116.164301](https://doi.org/10.1103/PhysRevLett.116.164301).
- Slob, E., K. Wapenaar, F. Brogini, and R. Snieder, 2014, Seismic reflector imaging using internal multiples with Marchenko-type equations: *Geophysics*, **79**, no. 2, S63–S76, doi: [10.1190/geo2013-0095.1](https://doi.org/10.1190/geo2013-0095.1).
- Staring, M., M. Dukalski, M. Belonosov, R. H. Baardman, J. Yoo, R. F. Hegge, R. van Borselen, and K. Wapenaar, 2021, Robust estimation of

- primaries by sparse inversion and Marchenko equation-based workflow for multiple suppression in the case of a shallow water layer and a complex overburden: A 2D case study in the Arabian Gulf: *Geophysics*, **86**, no. 2, Q15–Q25, doi: [10.1190/geo2020-0204.1](https://doi.org/10.1190/geo2020-0204.1).
- Staring, M., R. Pereira, H. Douma, J. van der Neut, and K. Wapenaar, 2018, Source-receiver Marchenko redatuming on field data using an adaptive double-focusing method: *Geophysics*, **83**, no. 6, S579–S590, doi: [10.1190/geo2017-0796.1](https://doi.org/10.1190/geo2017-0796.1).
- Staring, M., and K. Wapenaar, 2020, Three-dimensional Marchenko internal multiple attenuation on narrow azimuth streamer data of the Santos Basin, Brazil: *Geophysical Prospecting*, **68**, 1864–1877, doi: [10.1111/1365-2478.12964](https://doi.org/10.1111/1365-2478.12964).
- Taner, M. T., 1976, Simplan: Simulated plane-wave exploration: 46th Annual International Meeting, SEG, Expanded Abstracts, 186–187.
- ten Kroode, F., 2002, Prediction of internal multiples: *Wave Motion*, **35**, 315–338, doi: [10.1016/S0165-2125\(01\)00109-3](https://doi.org/10.1016/S0165-2125(01)00109-3).
- Thorbecke, J., L. Zhang, K. Wapenaar, and E. Slob, 2021, Implementation of the Marchenko multiple elimination algorithm: *Geophysics*, **86**, no. 2, F9–F23, doi: [10.1190/geo2020-0196.1](https://doi.org/10.1190/geo2020-0196.1).
- Ursin, B., 1983, Review of elastic and electromagnetic wave propagation in horizontally layered media: *Geophysics*, **48**, 1063–1081, doi: [10.1190/1.1441529](https://doi.org/10.1190/1.1441529).
- van Borselen, R., 2002, Fast-track, data-driven interbed multiple removal — A North Sea data example: 64th Annual International Conference and Exhibition, EAGE, Extended Abstracts, F–40, doi: [10.3997/2214-4609-pdb.5.F040](https://doi.org/10.3997/2214-4609-pdb.5.F040).
- van der Neut, J., J. L. Johnson, K. van Wijk, S. Singh, E. Slob, and K. Wapenaar, 2017, A Marchenko equation for acoustic inverse source problems: *Journal of the Acoustical Society of America*, **141**, 4332–4346, doi: [10.1121/1.4984272](https://doi.org/10.1121/1.4984272).
- van der Neut, J., J. Thorbecke, K. Mehta, E. Slob, and K. Wapenaar, 2011, Controlled-source interferometric redatuming by crosscorrelation and multidimensional deconvolution in elastic media: *Geophysics*, **76**, no. 4, SA63–SA76, doi: [10.1190/1.3580633](https://doi.org/10.1190/1.3580633).
- van der Neut, J., J. Thorbecke, K. Wapenaar, and E. Slob, 2015a, Inversion of the multidimensional Marchenko equation: 77th Annual International Conference and Exhibition, EAGE, Extended Abstracts, We–N106–04, doi: [10.3997/2214-4609.201412939](https://doi.org/10.3997/2214-4609.201412939).
- van der Neut, J., I. Vasconcelos, and K. Wapenaar, 2015b, On Green's function retrieval by iterative substitution of the coupled Marchenko equations: *Geophysical Journal International*, **203**, 792–813, doi: [10.1093/gji/ggv330](https://doi.org/10.1093/gji/ggv330).
- van der Neut, J., K. Wapenaar, J. Thorbecke, E. Slob, and I. Vasconcelos, 2015c, An illustration of adaptive Marchenko imaging: *The Leading Edge*, **34**, 818–822, doi: [10.1190/le34070818.1](https://doi.org/10.1190/le34070818.1).
- van der Neut, J., and K. Wapenaar, 2016, Adaptive overburden elimination with the multidimensional Marchenko equation: *Geophysics*, **81**, no. 5, T265–T284, doi: [10.1190/geo2016-0024.1](https://doi.org/10.1190/geo2016-0024.1).
- van Groenestijn, G. J. A., and D. J. Verschuur, 2010, Estimation of primaries by sparse inversion from passive seismic data: *Geophysics*, **75**, no. 4, SA61–SA69, doi: [10.1190/1.3460431](https://doi.org/10.1190/1.3460431).
- van IJsseldijk, J., and K. Wapenaar, 2021, Adaptation of the iterative Marchenko scheme for imperfectly sampled data: *Geophysical Journal International*, **224**, 326–336, doi: [10.1093/gji/ggaa463](https://doi.org/10.1093/gji/ggaa463).
- Vasconcelos, I., and Y. Sripanich, 2019, Scattering-based Marchenko for subsurface focusing and redatuming in highly complex media: 81st Annual International Conference and Exhibition, EAGE, Extended Abstracts, Tu–R04–06, doi: [10.3997/2214-4609.201900829](https://doi.org/10.3997/2214-4609.201900829).
- Vasconcelos, I., K. Wapenaar, J. van der Neut, C. Thomson, and M. Ravasi, 2015, Using inverse transmission matrices for Marchenko redatuming in highly complex media: 85th Annual International Meeting, SEG, Expanded Abstracts, 5081–5086, doi: [10.1190/segam2015-5896301.1](https://doi.org/10.1190/segam2015-5896301.1).
- Verschuur, D. J., and A. J. Berkhout, 2005, Removal of internal multiples with the common-focus-point (CFP) approach — Part 2: Application strategies and data examples: *Geophysics*, **70**, no. 3, V61–V72, doi: [10.1190/1.1925754](https://doi.org/10.1190/1.1925754).
- Verschuur, D. J., A. J. Berkhout, and C. P. A. Wapenaar, 1992, Adaptive surface-related multiple elimination: *Geophysics*, **57**, 1166–1177, doi: [10.1190/1.1443330](https://doi.org/10.1190/1.1443330).
- Wapenaar, C. P. A., 1996, One-way representations of seismic data: *Geophysical Journal International*, **127**, 178–188, doi: [10.1111/j.1365-246X.1996.tb01543.x](https://doi.org/10.1111/j.1365-246X.1996.tb01543.x).
- Wapenaar, C. P. A., N. A. Kinneging, and A. J. Berkhout, 1987, Principle of prestack migration based on the full elastic two-way wave equation: *Geophysics*, **52**, 151–173, doi: [10.1190/1.1442291](https://doi.org/10.1190/1.1442291).
- Wapenaar, K., 2003, Synthesis of an inhomogeneous medium from its acoustic transmission response: *Geophysics*, **68**, 1756–1759, doi: [10.1190/1.1620649](https://doi.org/10.1190/1.1620649).
- Wapenaar, K., J. Brackenhoff, and J. Thorbecke, 2019, Green's theorem in seismic imaging across the scales: *Solid Earth*, **10**, 517–536, doi: [10.5194/se-10-517-2019](https://doi.org/10.5194/se-10-517-2019).
- Wapenaar, K., and E. Slob, 2014, On the Marchenko equation for multicomponent single-sided reflection data: *Geophysical Journal International*, **199**, 1367–1371, doi: [10.1093/gji/ggu313](https://doi.org/10.1093/gji/ggu313).
- Wapenaar, K., J. Thorbecke, J. van der Neut, F. Brogini, E. Slob, and R. Snieder, 2014, Green's function retrieval from reflection data, in absence of a receiver at the virtual source position: *Journal of the Acoustical Society of America*, **135**, 2847–2861, doi: [10.1121/1.4869083](https://doi.org/10.1121/1.4869083).
- Ware, J. A., and K. Aki, 1969, Continuous and discrete inverse-scattering problems in a stratified elastic medium — Part 1: Plane waves at normal incidence: *Journal of the Acoustical Society of America*, **45**, 911–921, doi: [10.1121/1.1911568](https://doi.org/10.1121/1.1911568).
- Weglein, A. B., F. V. Araújo, P. M. Carvalho, R. H. Stolt, K. H. Matson, R. T. Coates, D. Corrigan, D. J. Foster, S. A. Shaw, and H. Zhang, 2003, Inverse scattering series and seismic exploration: *Inverse Problems*, **19**, R27–R83, doi: [10.1088/0266-5611/19/6/R01](https://doi.org/10.1088/0266-5611/19/6/R01).
- Weglein, A. B., F. A. Gasparotto, P. M. Carvalho, and R. H. Stolt, 1997, An inverse-scattering series method for attenuating multiples in seismic reflection data: *Geophysics*, **62**, 1975–1989, doi: [10.1190/1.1444298](https://doi.org/10.1190/1.1444298).
- Zhang, L., and E. Slob, 2020a, A fast algorithm for multiple elimination and transmission compensation in primary reflections: *Geophysical Journal International*, **221**, 371–377, doi: [10.1093/gji/ggaa005](https://doi.org/10.1093/gji/ggaa005).
- Zhang, L., and E. Slob, 2020b, A field data example of Marchenko multiple elimination: *Geophysics*, **85**, no. 2, S65–S70, doi: [10.1190/geo2019-0327.1](https://doi.org/10.1190/geo2019-0327.1).
- Zhang, L., J. Thorbecke, K. Wapenaar, and E. Slob, 2019a, Data-driven internal multiple elimination and its consequences for imaging: A comparison of strategies: *Geophysics*, **84**, no. 5, S365–S372, doi: [10.1190/geo2018-0817.1](https://doi.org/10.1190/geo2018-0817.1).
- Zhang, L., J. Thorbecke, K. Wapenaar, and E. Slob, 2019b, Transmission compensated primary reflection retrieval in the data domain and consequences for imaging: *Geophysics*, **84**, no. 4, Q27–Q36, doi: [10.1190/geo2018-0340.1](https://doi.org/10.1190/geo2018-0340.1).



Kees Wapenaar received a Ph.D. (1986, cum laude) in applied physics at Delft University of Technology (TU Delft), the Netherlands. From 1986 until 1999, he was associate professor and co-project leader of the Delphi research consortium in the Department of Applied Physics at TU Delft. In 1999, he was appointed Antoni van Leeuwenhoek Professor in the Department of Geoscience and Engineering. Since 2002, he has been head of the geophysics and petrophysics research group at that department. His research interests include wave theory and its applications in seismic imaging and interferometric methods. He received SEG's best paper in GEOPHYSICS award (2006), the Virgil Kauffman Gold Medal (2010), EAGE's Conrad Schlumberger Award (2013), and an ERC Advanced Grant from the European Union (2016). From 2007 until 2009, he served as editor in chief of GEOPHYSICS.



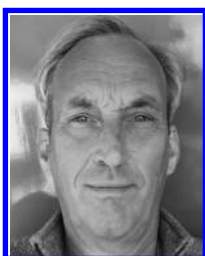
Joeri Brackenhoff received a B.S. (2014, cum laude) in applied earth sciences from Delft University, an M.S. (2016, cum laude) in applied geophysics from the IDEA League, and a Ph.D. (2021) in applied geophysics from TU Delft. Since 2021, he has been working as a postdoctoral fellow at the Seismology and Wave Physics groups of ETH Zürich. His research interests include the study of wave physics for the purpose of seismic imaging and inversion. He is a board member of the EAGE local chapter in the Netherlands and is a member of the SEG, EAGE, and AGU.



Giovanni Angelo Meles received an M.S. (2004) in physics from the Università Statale di Milano, Milan, Italy. In 2007, he moved to Zürich, where in 2011 he earned a Ph.D. from the Swiss Federal Institute of Technology (ETH) under the supervision of A. Green, S. Greenhalgh, and J. van der Kruk. From September 2011 to December 2016, he was with the Edinburgh Interferometry Project at the University of Edinburgh, Edinburgh, U.K., where he conducted research in close contact with A. Curtis. In February 2017, he became part of K. Wapenaar's group at TU Delft, working mainly on Marchenko plane-wave methods and focusing strategies. He has been working with N. Linde from the University of Lausanne since December 2020. His research interests include GPR/seismic imaging, full-waveform inversion, and focusing strategies.



Chris Reinicke received a B.S. (2013) from the Technical University of Munich and an M.S. (2015) in applied geophysics from the IDEA League (TU Delft, ETH Zürich, RWTH Aachen). Next, he started his Ph.D. research on the elastodynamic Marchenko method under the supervision of K. Wapenaar at TU Delft. After graduation in 2020, he continued his work on Marchenko-equation-based multiple elimination as a researcher at Aramco's Global Research Center in Delft. His main research interests include multiples, inverse problems, and advanced seismic data processing. He has been a member of SEG and EAGE since 2015.



Evert Slob received a doctorate degree (1994, cum laude) in applied sciences from Delft University of Technology (TU Delft), the Netherlands. From 1995 to 2011, he was a research fellow, assistant, and associate professor, and since 2011, he has been a professor in the Department of Geosciences and Engineering at TU Delft. He was the general chair of the 10th International Conference on GPR in 2004. He was the SEG editor from 2013 to 2015. He served as a director of education of civil engineering and geosciences from 2014 to 2018. He has organized more than a dozen international workshops and conference sessions and was guest editor for 12 special journal issues on different topics including GPR and hydrogeophysics. He is a coauthor of *Introduction to Controlled-Source Electromagnetic Methods* published in 2019. He is a coeditor of *Seismoelectric Exploration* published in 2021. He received the Reginald Fessenden Award from SEG in 2020. His research interests include wavefield processing, imaging, and inversion. He is a member of EAGE and SEG.



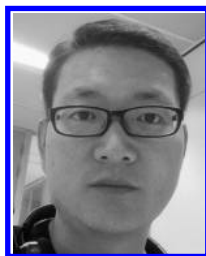
Myrna Staring received a B.S. from the University College Roosevelt and an M.S. in applied geophysics from the IDEA League (TU Delft, ETH Zürich, RWTH Aachen). In September 2020, she also received her doctorate degree in applied geophysics from TU Delft. She works at Fugro Innovation and Technology as a technologist specializing in active and passive seismic technologies for near-surface characterization. Her research interest is in the practical application of novel seismic technologies that can improve seismic imaging and inversion. She is passionate about diversity and inclusion and is the president of GAIA and EAGE Women in Geoscience and Engineering Netherlands.



Jan Thorbecke received an M.S. (1991) in applied earth sciences and a Ph. D. (1997) in applied physics at TU Delft. Since 1997, he has worked at Cray as an application and performance engineer in high-performance computing. In 2020, he became a distinguished technologist at HPE-Cray and works as a performance engineer on the optimization and parallelization of computationally intensive scientific applications. Since 2002, he has also been working (0.2 fte) at TU Delft as a senior researcher on the development of new imaging algorithms. His research interest is in the design and implementation of imaging, modeling, and data processing algorithms.



Joost van der Neut received a doctorate degree (2012, cum laude) in applied geophysics from TU Delft. In 2013, he received a Veni personal grant from the Dutch Research Council (NWO). In 2017, he started a postdoc at the Department of Applied Sciences (TU Delft), and he continued with another postdoc at the Department of Geosciences and Engineering (TU Delft) in 2021. He received a best student presentation award (SEG, 2009), a best presentation award (SEG, 2010), a J. Clarence Karcher Award (SEG, 2015), and a best paper award (*Geophysical Prospecting*, 2016). His research interests include wave propagation, imaging, and inversion.



Lele Zhang received a doctorate degree (2019) in applied sciences from TU Delft. Since the beginning of 2020, he has worked as a postdoctoral research fellow in the Department of Geosciences and Engineering at TU Delft. He has organized several international workshops and conference sessions and was guest editor for one special journal issue on multiple reflections in *GEOPHYSICS*. His research interests include signal processing, wavefield propagation, and migration.